MAX-PLANCK-INSTITUT FÜR PLASMAPHYSIK

GARCHING BEI MÜNCHEN

SIMNRA User's Guide

Matej Mayer

IPP 9/113 **April 1997**

Die nachstehende Arbeit wurde im Rahmen des Vertrages zwischen dem Max-Planck-Institut für Plasmaphysik und der Europäischen Atomgemeinschaft über die Zusammenarbeit auf dem Gebiete der Plasmaphysik durchgeführt.

April 1997

Abstract

This report describes the use of the program SIMNRA and the physical concepts implemented therein. SIMNRA is a Microsoft Windows 95 / Windows NT program for the simulation of back- or forward scattering spectra for ion beam analysis with MeV ions. SIMNRA is mainly intended for the simulation of spectra with non-Rutherford backscattering cross-sections, nuclear reactions and elastic recoil detection analysis (ERDA). About 300 different non-Rutherford and nuclear reaction cross-sections for incident protons, deuterons, ^{3}He and ^{4}He-ions are included. SIMNRA can calculate spectra for any ion-target combination including incident heavy ions and any geometry including arbitrary foils in front of the detector. SIMNRA uses the Andersen-Ziegler values for the stopping powers of swift and heavy ions and Chu energy loss straggling. Additionally SIMNRA can calculate the effects of dual scattering. Data fitting (layer thicknesses, compositions etc.) is possible by means of the Simplex algorithm.

This manual describes SIMNRA version 3.0

Contents

1 Overview **1**

2 Installation **3**

2.1 System requirements 3

2.2 Installation 3

3 Using SIMNRA **5**

3.1 Basic steps 5

3.2 The `File` menu 7

3.3 The `Edit` menu 9

3.4 The `Setup` menu 10

3.4.1 `Setup:Experiment...` 10

3.4.2 `Setup:Calculation...` 12

3.5 The `Target` menu 15

3.5.1 `Target:Target...` 15

3.5.2 `Target:Foil...` 17

3.6 The `Reactions` menu 18

3.7 The `Calculate` menu 26

3.7.1 `Fit Spectrum...` 26

3.8 The `Plot` menu 28

3.9 The `Options` menu 29

3.10 Adding new cross-section data 30

3.10.1 The R33 file format 30

3.11 Detector nonlinearity 33

4 Physics **34**

4.1 Overview . . . 34

4.2 Cross-sections . . . 36

4.2.1 Rutherford cross-sections . . . 36

4.2.2 Non-Rutherford cross-sections . . . 37

4.3 Evaluation of energy loss . . . 38

4.4 Stopping power data . . . 40

4.4.1 Hydrogen . . . 40

4.4.2 Helium . . . 40

4.4.3 Heavy ions . . . 42

4.4.4 Stopping in compounds . . . 42

4.5 Straggling . . . 43

4.5.1 Electronic and nuclear energy loss straggling . . . 45

4.5.2 Energy loss straggling in compounds . . . 52

4.6 Multiple and plural scattering . . . 52

5 Examples **55**

5.1 RBS: Rutherford cross-sections . . . 55

5.2 RBS: Non-Rutherford cross-sections . . . 58

5.3 ERDA: Non-Rutherford cross-sections . . . 60

Chapter 1

Overview

This report describes the use of the program SIMNRA and the physical concepts implemented therein. SIMNRA is a Microsoft Windows 95 / Windows NT program for the simulation of back- or forward scattering spectra for ion beam analysis with MeV ions. SIMNRA is mainly intended for the simulation of spectra with non-Rutherford backscattering cross-sections, nuclear reactions and elastic recoil detection analysis (ERDA). About 300 different non-Rutherford and nuclear reaction cross-sections for incident protons, deuterons, ^{3}He and ^{4}He-ions are included. SIMNRA can calculate spectra for any ion-target combination including incident heavy ions and any geometry including arbitrary foils in front of the detector. SIMNRA uses the Andersen-Ziegler values for the stopping powers of swift and heavy ions and Chu energy loss straggling. Additionally SIMNRA can calculate the effects of dual scattering. Data fitting (layer thicknesses, compositions etc.) is possible by means of the Simplex algorithm.

In contrast to other programs for the simulation of backscattering spectra SIMNRA is easy to use due to the Microsoft Windows user interface. SIMNRA makes full use of the graphics capacities of Windows.

This manual is organised in the following way:

- System requirements and the installation of the program are described in chapter 2.
- The use of the program is described in chapter 3. A quick overview about the steps necessary to calculate a spectrum is given in chapter 3.1. More details are found in the rest of chapter 3.

- The physical concepts implemented in the program are described in detail in chapter 4.
- Some examples for the abilities of the program are shown in chapter 5.

Chapter 2

Installation

2.1 System requirements

SIMNRA is a native 32-bit program for Windows 95 or Windows NT and requires at least a 386-processor with math coprocessor or a higher processor (486, Pentium). A fast processor (100 MHz 486 or higher) is highly recommended. SIMNRA will run under Windows 3.1 with WIN32S Version 1.30 or higher[1]. However, using SIMNRA with Windows 3.1 is not recommended and may result in global protection faults. SIMNRA does not run under OS/2 Warp 3. Super-VGA resolution of 800×600 pixels or higher is recommended. SIMNRA requires about 2 MB free hard disk space. At least 8 MB RAM are recommended.

2.2 Installation

Unzip the file SIMNRAxy.ZIP[2] into a directory of your choice, for example C:\SIMNRA. Use pkunzip's -d switch to create the correct subdirectory structure. After unzipping you should have obtained the files listed in table 2.1.

Now run the program SIMNRA. The name of the executable program is SIMNRA.EXE. When you run SIMNRA for the first time, you will be prompted for the name of the directory where SIMNRA is installed, for the above example enter C:\SIMNRA. The names

[1] WIN32S is a 32-bit extension for Windows 3.1. It is available from Microsoft (http://www.microsoft.com). WIN32S is not needed for Windows 95 or Windows NT. SIMNRA will not run with WIN32S Version 1.25 or lower.

[2] xy is the version number, 30 stands for version 3.0

Directory	Files	
	SIMNRA.EXE	executable program
	README	Readme file
	MANUAL.PS	This manual
\ATOM	ATOMDATA.DAT	atomic data
\STOP	STOPH.DAT	stopping data
	STOPHE.DAT	
	LCORRHI.DAT	
	CHU_CORR.DAT	
\CRSEC	CRSDA.DAT	cross-section data
	*.R33	
	*.RTR	
\SAMPLES	*.NRA	examples

Table 2.1: Directory structure and files used by SIMNRA.

of the sub-directories will be created automatically.

Note: If you encounter error messages (File not found), then check the entries in `Options:Directories...`.

Chapter 3

Using SIMNRA

3.1 Basic steps

This section gives a quick overview about the basic steps necessary to calculate a backscattering spectrum.

Three steps must be performed before a backscattering spectrum can be calculated: In a first step the experimental situation (incident ions, geometry) has to be defined, then the target must be created, and in a third step the cross-sections used for the calculation have to be chosen.

1. Click `Setup:Experiment`. Here you choose the incident ions, the ions energy, define the scattering geometry (see fig. 3.2), and you enter the energy calibration of the experiment.

2. Click `Target:Target`. Here you create the target. Each target consists of *layers*. Each layer consists of different elements with some atomic concentration, which does not change throughout the layer, and each layer has a thickness.

3. If there is a foil in front of the detector, then click `Target:Foil` for the definition of a foil. The default is no foil in front of the detector. Like the target, the foil can consist of different layers, and the layers can have different compositions.

4. Click `Reactions`. Here you have to choose which cross-section data should be used for the simulation. The default are Rutherford cross-sections for all elements. You can select non-Rutherford cross-sections instead and you can add nuclear reactions.

5. Now the spectrum can be calculated. Click `Calculate:Calculate Spectrum` for a simulation of the spectrum.

6. With `Setup:Calculation` the parameters for the calculation can be altered. The default values are normally sufficient, and you should change these values only if you know what you are doing.

7. With `File:Read data` a measured spectrum can be imported for comparison with the simulated one and for data fitting.

3.2 The `File` menu

In the `File` menu all necessary commands for reading and saving files and data, printing spectra and terminating the program are located.

- `New`: This menu item resets the program to its starting values. All calculated spectra, target, foil and setup definitions will be deleted.

- `Open...`: This menu item will read a saved calculation from disk.

- `Save`: This menu item will save all current parameters, target and foil definitions, experimental and simulated data to disk. The data are saved as an ASCII file. The default file extension is NRA.

- `Save as...`: Like `Save`, but you will be prompted for the name of the file.

- `Read Data`: This menu item allows the import of experimental data.

  `Read Data:IPP...`: Reads experimental data stored in the data file format used at the IPP Garching. This data file format will not be described here.

  `Read Data:ASCII...`: Allows the import of experimental data in ASCII format.

  The data file format must be as follows: The file may contain an arbitrary number of comment lines at the beginning of the file. A comment line is a line that contains any non-numeric character. These lines will be ignored. The first line that contains only numeric characters will be treated as the first line of data. Each data line must consist of two columns: In the first column the channel number must be given (Integer), in the second column the number of counts must be given (Double). The two columns are separated by an arbitrary number of blanks or tabs. Each line must end with <CR><LF>[1]. The data file may contain up to 8192 channels. An example for a valid data file is given in fig. 3.1.

- `Write Data...`: This menu item exports the experimental and simulated data as columns into an ASCII file. You can import this file easily into any plot program, such as Excel, Origin or Mathematica.

[1] <CR> means Carriage Return (#13 decimal), <LF> means Line Feed (#10 decimal).

```
This line may contain any comment <CR><LF>
This line may contain any comment as well <CR><LF>
 Channel  Counts <CR><LF>
       1    1000 <CR><LF>
       2  1000.0 <CR><LF>
       3   1.0E3 <CR><LF>
       4  +1.0E3 <CR><LF>
  <EOF>
```

Figure 3.1: Example for a valid data file which can be imported with `File:Read Data:ASCII...`. The first three lines will be ignored by the program. The channel number must be an integer number, counts may be integer or floating point numbers.

The file format is as follows: The first line is a comment line which contains information about the contents of the different columns. The first column is the channel number, the second column contains the experimental data (This column is set to zero if experimental data are not available), the third column contains the simulated data (This column is set to zero if simulated data are not available). If the `Element spectra` option in `Setup:Calculation...` is checked, then the next columns will contain the simulated spectra for each element in the target. The columns are separated with blanks.

- `Print...`: This menu item will print all parameters of the calculation and plot the experimental and simulated curves.

  Note 1: SIMNRA is not intended to produce high quality graphics, and the plot looks quite ugly. If you want to obtain high quality graphics, you should use a graphics program such as Excel or Origin. You can exchange data between SIMNRA and any graphics program by file with `File:Write Data...` and via the clipboard with `Edit:Copy Data`.

  Note 2: Printing may not work properly if the program is used under Windows 3.1. Printing works properly under Windows 95 and Windows NT.

- `Exit`: Terminates the program.

3.3 The `Edit` menu

- `Copy Data`: This will copy the experimental and simulated data in ASCII format to the clipboard. They can be pasted into any spreadsheet program.

  The format of the data in the clipboard is as follows: The data are organised in three columns. The first column contains the channel number, the second column contains the experimental data, and the third column contains the simulated data. The columns are separated with tabs.

  Note 1: SIMNRA does not support OLE.

  Note 2: `Copy Data` does not work properly under Windows 3.1 and is disabled. `Copy Data` works properly under Windows 95 and Windows NT.

3.4 The `Setup` menu

3.4.1 `Setup:Experiment...`

In the `Setup:Experiment...` menu the global parameters of the backscattering experiment are defined.

- `Incident ion`: Selects the incident ions. For incident protons (H), D, T, ^{3}He or ^{4}He ions, the ions are selected by clicking the appropriate radio button.

  For incident heavy ions select `Other` and enter the ions name in `Other ion:Element` (for example Si, Cl, I). Lowercase and uppercase letters in the ions name are treated similar, you can enter silicon as Si, si, SI or sI. The ions mass is selected from the drop down box.

- `Energy`: Energy of the incident ions (in keV).

- `Geometry`: Geometry of the experiment: Incident angle α, exit angle β and scattering angle θ. α and β are measured towards the surface normal, see fig 3.2. All angles in degrees.

  Note: $0° \leq \beta < 90°$. Transmission geometry is not possible.

- `Calibration`: Conversion from channels to energy. To account for detector nonlinearities, SIMNRA can use a non-linear energy calibration with a quadratic term of the form

$$E\,[\text{keV}] = A + B \times \text{channel} + C \times \text{channel}^2. \tag{3.1}$$

  E is the particle energy in keV. The calibration offset A must be entered in the `Calibration Offset` field, A in keV. The energy per channel B must be entered in the `Energy per Channel` field, B in keV/channel. C is the quadratic correction term, C in keV/channel^2. For a linear energy calibration $C = 0.0$. A linear calibration is appropriate in most cases, and only if a high accuracy is intended a non-linear calibration should be used.

  Attention: If a non-linear energy calibration is used, then the energy scale, which is plotted at the top axis, is only approximately valid: This scale remains linear even for non-linear energy calibrations.

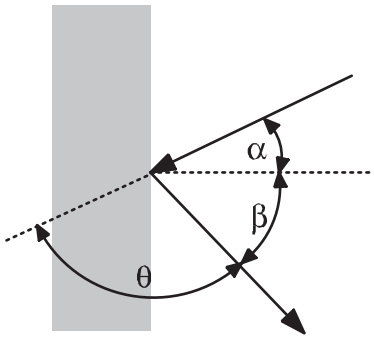

Figure 3.2: Geometry of a scattering experiment. Incident angle α, exit angle β and scattering angle θ.

- `Particles*sr`: Number of incident particles times the solid angle of the detector. Solid angle in steradians.

- `Detector Resolution`: Energy resolution of the detector (in keV). The energy resolution is measured as full width at half maximum (FWHM).

- `Energy spread of incident beam`: Usually the incident ion beam is not monoenergetic but has an energy distribution. SIMNRA assumes a gaussian energy distribution of the incident beam with a full width at half maximum which can be entered in the `Energy spread of incident beam` field. The energy distribution of the incident beam depends on the experimental setup, typical values for this energy spread are several keV in many experiments. If this field is set to 0.0 SIMNRA assumes a monoenergetic incident beam.

3.4.2 `Setup:Calculation...`

In the `Setup:Calculation...` menu the parameters for the calculation can be altered. This affects the accuracy of the calculation, but also the time necessary for the calculation of a simulated spectrum.

- `Stepwidth incoming ion`: Stepwidth of the incoming ion (in keV). See chapter 4 for details. The default is 10 keV. The stepwidth of the incoming ion affects the time T necessary to perform a calculation heavily. T depends on the stepwidth of the incoming ion ΔE roughly as $T \propto 1/\Delta E$: Decreasing the stepwidth by a factor of two will roughly double the computing time.

  For incident heavy ions with energies in the range of several ten MeV you can increase this stepwidth to several 100 keV.

  Note 1: The stepwidth of the incident ions is an important parameter for the accuracy of a simulation. If the stepwidth of the incident ion is too high, especially if the exit angle β is close to 90° or the detector resolution is below 10 keV, unwanted oscillations or steps in the simulated spectra may occur. This is due to rounding errors in the routine which calculates the contents of each channel. If these oscillations occur you have to decrease the stepwidth of the incident ion.

  Note 2: If the backscattering cross-section contains narrow resonances, the stepwidth of the incoming ions should be lower than the width of the resonance.

- `Stepwidth Outgoing Particle`: Stepwidth of outgoing particles (in keV). See chapter 4 for details. The default is 200 keV.

- `Cutoff Energy`: All particles are calculated until their energy has decreased below the cut-off energy. You may speed up the calculation if you increase the cut-off energy. The lowest possible value for the cut-off energy is 10 keV.

- `Isotopes`: If checked, backscattering from all isotopes of all elements in the target is calculated. Especially for heavy elements with many isotopes this will slow down the calculation significantly. If unchecked, the program will use only the mean masses of the elements. Default is checked.

  Important: Non-Rutherford cross-sections and nuclear reactions are only available if `Isotopes` is checked.

- `Straggling`: If checked, electronic and nuclear energy loss straggling will be taken into account. Default is checked.

  Note: Straggling due to multiple small angle scattering is not calculated by the program. See chapter 4 for details.

- `High energy stopping`: If checked, the program will use the high energy stopping formula by Andersen and Ziegler for incident protons and heavy ions for $E >$ 1 MeV/amu. If unchecked, the program will use the medium energy formula, which is valid only in the range 10 keV/amu–1 MeV/amu, also at higher energies $E > 1$ MeV/amu. The difference between the two formulas is very small in most cases. This switch does not have any influence on the calculation of the stopping power of helium ions and is disabled. For helium ions always the medium energy formula is used, which is valid for all energies below 10 MeV. The default is checked.

  Note: If you use high energy stopping, you may obtain kinks in the spectra because the two stopping power formulas do not fit absolutely smoothly together: The derivative of the stopping power jumps at 1 MeV/amu.

- `Dual Scattering`: Most particles are scattered into the detector with only one scattering event with large scattering angle. However, some particles may suffer more than one scattering event with large scattering angle before they reach the detector, see fig. 3.3. This is called plural scattering and results for example in the low background behind the low energy edge of high Z layers on top of low Z elements. The deviations at low energies between simulated and measured spectra are also mainly due to plural scattering.

  SIMNRA can calculate all trajectories with two scattering events. If `Dual Scattering` is unchecked, then only one scattering event is calculated. This is the default. If `Dual Scattering` is checked, additionally trajectories with two scattering events will be calculated.

  Warning: The calculation of dual scattering is a very time consuming process. If `Dual Scattering` is checked, this will slow down the calculation of a spectrum by a factor of about 200 (!), increasing the computing time from several seconds to *at least* several minutes.

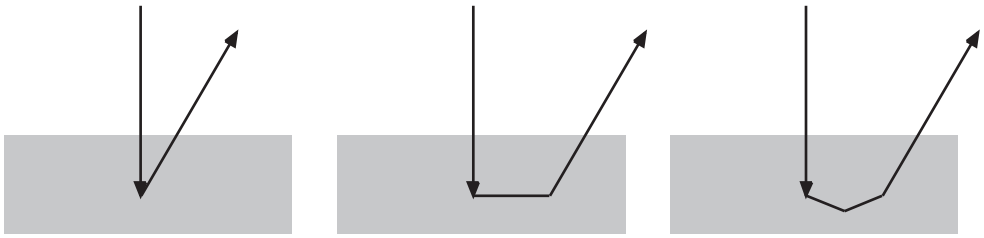

Figure 3.3: Examples of ion trajectories with one, two and three scattering events.

Note 1: Dual scattering should be used *only* if all cross-sections are Rutherford. For the calculation of dual scattering the cross-sections for all possible scattering angles between $\approx 0°$ and $180°$ must be known. This is only the case for Rutherford cross-sections.

Note 2: SIMNRA calculates dual scattering *only* for incident ions and not for recoils or reaction products of nuclear reactions. Additional scattering in a foil in front of the detector (if any) is neglected.

Note 3: If `Dual Scattering` is checked, then `Straggling` must be checked too. SIMNRA will check `Straggling` automatically, if `Dual Scattering` is checked. As long as `Dual Scattering` is checked, `Straggling` cannot be unchecked.

- `Element Spectra`: If checked, individual spectra for each element in the target will be calculated and plotted. If unchecked, only the total spectrum will be calculated and plotted. Default is unchecked.

- `Logfile`: If checked, a file named SIMNRA.LOG will be created. This file contains additional information about each step of the calculation. The logfile is intended for debugging the program. Default is unchecked.

3.5 The `Target` menu

3.5.1 `Target:Target...`

In this menu the target is created. A target consists of *layers*. Each layer consists of different elements and has some thickness. The composition of a layer does not change throughout his thickness. To simulate a concentration profile you have to use multiple layers.

The layer number 1 is at the surface of the target, the layer number 2 is below layer 1 and so on, see fig. 3.4.

- `Thickness`: Thickness of the layer (in 10^{15} atoms/cm^2).
- `Number of Elements`: Number of different elements in this layer. The maximum number of different elements in a layer is 20.
- `Element`: Name of the element, for example Si, W, Au. Lowercase and uppercase letters in elements names are treated similar, you can enter silicon as Si, si, SI or sI. XX means that this element is unknown. The special symbols D for deuterium, T for tritium and A for ^{4}He can be used.
- `Concentration`: Atomic concentration of the element in the actual layer. The concentration c must be $0.0 \leq c \leq 1.0$. The sum of the concentrations of all elements in one layer must be equal to 1 ($0.999 \leq \sum c_i \leq 1.001$). If the sum of concentrations is not equal to 1, the word concentration is written in red colour, if the sum of concentrations is equal to 1, the word concentration is written in black colour. You can use the small buttons to set the concentration of the element i to 1 minus the sum of concentrations of all other elements, $c_i = 1 - \sum_{i \neq j} c_j$.
- Isotopes: You can use these buttons to change the concentrations of isotopes of that element in the actual layer. You will need this only if this element does not have the natural composition of isotopes. You can create for example a layer of enriched ^{13}C on top of ^{12}C, or the like. The sum of concentrations of all isotopes of one element must be equal to 1.

  Note: The `Isotopes` check-box in the `Setup:Calculation...` menu must be checked to manipulate individual isotopes.

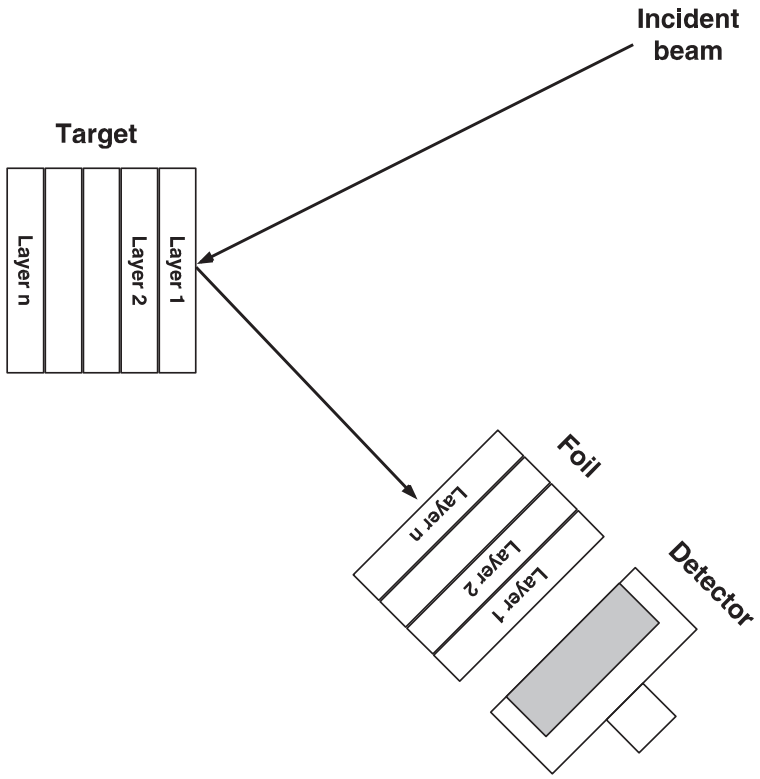

Figure 3.4: Layer structure of target and foil. For the target, layer 1 is at the surface, the layer with the highest number is the deepest layer. Backscattered particles first penetrate the foil layer with the highest number, the foil layer 1 is in front of the detector.

To manipulate layers use the buttons in the `Layer manipulation` box.

- `Add`: Adds a layer. The added layer will be the last layer. The maximum number of different layers is 100.
- `Ins`: Inserts a layer in front of the current layer. The maximum number of different layers is 100.
- `Del`: Deletes the current layer.
- `Prev`: Go to the previous layer.
- `Next`: Go to the next layer.

A layer can be copied to the clipboard with `Edit:Copy Layer` (or by pressing Ctrl C). A layer can be pasted from the clipboard with `Edit:Paste Layer` (or by pressing Ctrl V). **Attention:** If a layer is pasted, the current layer is overwritten.

3.5.2 `Target:Foil...`

In this menu a foil in front of the detector can be created. Like the target a foil can consist of multiple layers with different compositions. See the previous section for details. If the foil consists of multiple layers, then backscattered particles first will penetrate layer n, then layer $n-1$ etc., layer 1 is directly in front of the detector (see fig. 3.4).

The default is no foil in front of the detector.

3.6 The `Reactions` menu

In the `Reactions` menu the cross-sections used for the calculation of the simulated spectrum are chosen. Rutherford cross-sections for backscattering of projectiles and creation of recoils are available for all ion-target combinations, if kinematically possible. Additionally SIMNRA can handle non-Rutherford cross-sections for backscattering and recoil production and can use nuclear reactions cross-sections. SIMNRA is able to read three different file formats with cross-section data:

1. The file CRSDA.DAT. This file was developed during the last years at the IPP Garching and contains fitting coefficients to various cross-section data. A documentation is not available, and no guarantee is provided that the fits agree with the original data. Data from this file should be used with care and only if no other data are available.

2. The R33 file format. Cross-sections for nuclear reaction are stored in the R33 file format in the SigmaBase data repository for ion beam analysis[2]. Most files with this extension have been taken from SigmaBase, a few ones were added by the author. The majority of these files has been digitised from the original publications by G. Vizkelethy from Idaho State University. No guarantee is provided for agreement with the original publication. The references of the original publications are found in the file headers.

3. The RTR (Ratio To Rutherford) file format. These files contain non-Rutherford cross-sections for backscattering of protons and α-particles. The files contain the ratio of measured to Rutherford cross-sections. The majority of the data has been digitised from the original publications by R.P. Cox, J.A. Leavitt and L.C. McIntyre, Jr. from Arizona University. These cross-section data have been published in [1]. All files with this extension have been taken from SigmaBase. The references of the original publications are found in [1].

SIMNRA distinguishes between three different types of scattering events for each isotope:

[2] http://ibaserver.physics.isu.edu/sigmabase. This server is mirrored in New Zealand at http://pixe.gns.cri.nz/.

1. Backscattering of projectiles

2. Creation of recoils

3. Nuclear reactions.

The chosen cross-sections for each type of scattering event must be unambiguous: You can choose, for example, Rutherford cross-section for backscattering in the energy range from 0.000–0.999 MeV, some non-Rutherford cross-section for backscattering in the energy range from 1.000-1.999 MeV and a different cross-section for backscattering in the energy range from 2.000–3.000 MeV. You cannot choose, however, Rutherford cross-section for backscattering in the range 0.000–2.000 MeV and another cross-section for backscattering in the energy range from 1.000–2.000 MeV: In this case the program does not know which cross-section it should use in the range from 1.000–2.000 MeV, and you will get the error message 'Energy overlap in cross-sections'.

All available cross-section data are listed in tables 3.1–3.3. If you want to add new cross-section data files, see section 3.10.

Note 1: Files containing total cross-sections in the R33 file format are ignored. SIMNRA currently handles only differential cross-section data.

Note 2: Use the data files that came with SIMNRA. Some of the original data files at SigmaBase contain small format errors, such as additional blank lines, which confuse the program.

Note 3: Non-Rutherford cross-sections and nuclear reactions are only available if `Isotopes` in the `Setup:Calculation...` menu is checked.

Table 3.1: Non-Rutherford backscattering cross-sections.

	θ **(Lab)**	**Energy (keV)**	**File**	**Reference**
D(p,p)D	151	1800–3000	PH_LA76A.RTR	Langley 1976
T(p,p)T	163.2	2500–3500	PH_LA76B.RTR	Langley 1976
^{3}He(p,p)^{3}He	159.2	2000–3000	PHELA76A.RTR	Langley 1976
^{4}He(p,p)^{4}He	161.4	1500–3700	PHELA76B.RTR	Langley 1976
^{4}He(p,p)^{4}He	165	1500–3000	CRSDA.DAT, No. 5	?
^{6}Li(p,p)^{6}Li	164	1200–3100	PLIBA51A.RTR	Bashkin 1951
^{7}Li(p,p)^{7}Li	156.7	373–1398	PLIWA53A.RTR	Warters 1953
^{7}Li(p,p)^{7}Li	164	1700–3500	PLIBA51B.RTR	Bashkin 1951
^{7}Li(p,p)^{7}Li	165	1300–2800	PLIMA56A.RTR	Malmberg 1956
^{9}Be(p,p)^{9}Be	142.4	1600–3000	PBEMO56A.RTR	Mozer 1956
^{9}Be(p,p)^{9}Be	158.7	200–1700	PBEMO56B.RTR	Mozer 1956
^{9}Be(p,p)^{9}Be	170.5	2400–2700	PBELE94A.RTR	Leavitt 1994
^{10}B(p,p)^{10}B	154	1000–3000	PB_OV62A.RTR	Overley 1962
^{11}B(p,p)^{11}B	150	500–2000	PB_TA56A.RTR	Trautfest 1956
C(p,p)C	165	1000–3500	12CPPC.R33	Amirikas 1993
C(p,p)C	170	300–700	PC_LI93A.RTR	Liu 1993
C(p,p)C	170	700–2800	PC_LI93B.RTR	Liu 1993
C(p,p)C	170	300–3000	PC_LI93C.RTR	Liu 1993
C(p,p)C	170	700–2500	PC_RA85A.RTR	Rauhala 1985
C(p,p)C	170	996–3498	PC_AM93A.RTR	Amirikas 1993
^{12}C(p,p)^{12}C	168.2	400–4500	PC_JA53A.RTR	Jackson 1953
^{14}N(p,p)^{14}N	150	800–1900	PN_TA56A.RTR	Tautfest 1956
^{14}N(p,p)^{14}N	152	1035–1075	PN_HA57A.RTR	Hagedorn 1957
^{14}N(p,p)^{14}N	152	1450–1625	PN_HA57B.RTR	Hagedorn 1957
^{14}N(p,p)^{14}N	152	650–1800	PN_HA57E.RTR	Hagedorn 1957
^{14}N(p,p)^{14}N	155.2	1850–3000	PN_LA67A.RTR	Lambert 1967
^{14}N(p,p)^{14}N	158.7	1735–1760	PN_HA57C.RTR	Hagedorn 1957
^{14}N(p,p)^{14}N	158.7	1785–1815	PN_HA57D.RTR	Hagedorn 1957
^{14}N(p,p)^{14}N	159.5	600–4000	PN_BA59A.RTR	Bashkin 1959
^{14}N(p,p)^{14}N	165	1850–3000	PN_LA67B.RTR	Lambert 1967
^{14}N(p,p)^{14}N	167.2	3600–4100	PN_OL58A.RTR	Olness 1958
^{14}N(p,p)^{14}N	170	1450–2300	PN_RA85A.RTR	Rauhala 1985
^{16}O(p,p)^{16}O	149.5	2450–2850	PO_GO65A.RTR	Gomes 1965
^{16}O(p,p)^{16}O	170	1000–3580	PO_AM93A.RTR	Amirikas 1993
^{19}F(p,p)^{19}F	150	2000–5000	PF_BO93A.RTR	Bogdanovic 1993
^{19}F(p,p)^{19}F	160	500–1300	PF_DE56A.RTR	Dearnaly 1956
^{19}F(p,p)^{19}F	160	1300–2064	PF_DE56B.RTR	Dearnaly 1956
^{19}F(p,p)^{19}F	160	500–1300	PF_DE56C.RTR	Dearnaly 1956
^{19}F(p,p)^{19}F	160	1300–1550	PF_DE56D.RTR	Dearnaly 1956
^{19}F(p,p)^{19}F	165	850–1010	PF_KN89A.RTR	Knox 1989
^{19}F(p,p)^{19}F	165	1000–1875	PF_KN89B.RTR	Knox 1989
^{19}F(p,p)^{19}F	165	1350–1550	PF_KN89C.RTR	Knox 1989
^{19}F(p,p)^{19}F	158.7	600–1800	PF_WE55A.RTR	Webb 1955
^{19}F(p,p)^{19}F	158.7	1300–1500	PF_WE55B.RTR	Webb 1955
^{20}Ne(p,p)^{20}Ne	166 (CM)	1500–2800	PNELA71A.RTR	Lambert 1971
^{23}Na(p,p)^{23}Na	156.5	550–1450	PNABA56A.RTR	Bauman 1956
^{24}Mg(p,p)^{24}Mg	164	400–4000	PMGMO51A.RTR	Mooring 1951
^{24}Mg(p,p)^{24}Mg	164	792–856	PMGMO51E.RTR	Mooring 1951
^{24}Mg(p,p)^{24}Mg	164	1466–1501	PMGMO51F.RTR	Mooring 1951
^{24}Mg(p,p)^{24}Mg	164	1642–1671	PMGMO51G.RTR	Mooring 1951
^{24}Mg(p,p)^{24}Mg	164	1991–2026	PMGMO51H.RTR	Mooring 1951
^{24}Mg(p,p)^{24}Mg	164	2393–2431	PMGMO51I.RTR	Mooring 1951

	θ (Lab)	Energy (keV)	File	Reference
^{24}Mg(p,p)^{24}Mg	170	700–2540	PMGRA88A.RTR	Rauhala 1988
^{27}Al(p,p)^{27}Al	170	1000–2450	PALRA89A.RTR	Rauhala 1989
^{28}Si(p,p)^{28}Si	167.2	1300–4000	PSIVO59A.RTR	Vorona 1959
Si(p,p)Si	170	1000–3580	PSIAM93A.RTR	Amirikas 1993
Si(p,p)Si	170	1470–2200	PSIRA85A.RTR	Rauhala 1985
^{31}P(p,p)^{31}P	165	1000–2000	PP_CO63A.RTR	Cohen-Ganouna 1963
^{32}S(p,p)^{32}S	167.4	1300–4000	PS_OL58A.RTR	Olness 1958
S(p,p)S	170	1500–2690	PS_RA88A.RTR	Rauhala 1988
Cl(p,p)Cl	150	2000–5000	PCLBO93A.RTR	Bogdanovic 1993
^{40}Ar(p,p)^{40}Ar	159.5	1800–3600	PARBK61A.RTR	Barnhard 1961
^{40}Ar(p,p)^{40}Ar	166 (CM)	1000–2000	PARCO63A.RTR	Cohen-Ganouna 1963
^{40}Ar(p,p)^{40}Ar	166 (CM)	1825–1950	PARCO63B.RTR	Cohen-Ganouna 1963
^{40}Ar(p,p)^{40}Ar	155	1750–2750	PARFR58A.RTR	Frier 1958
^{40}Ca(p,p)^{40}Ca	160	1800–3000	PCAWI74A.RTR	Wilson 1974
^{48}Ti(p,p)^{48}Ti	160	1800–2150	PTIPR72A.RTR	Prochnow 1972
^{48}Ti(p,p)^{48}Ti	160	2150–2500	PTIPR72B.RTR	Prochnow 1972
^{48}Ti(p,p)^{48}Ti	160	2500–2800	PTIPR72C.RTR	Prochnow 1972
^{48}Ti(p,p)^{48}Ti	160	2900–3040	PTIPR72D.RTR	Prochnow 1972
^{48}Ti(p,p)^{48}Ti	170	1000–2600	PTIRA89A.RTR	Rauhala 1989

^{6}Li(α,α)^{6}Li	112	2500–4500	ALIBO72A.RTR	Bohlen 1972
^{7}Li(α,α)^{7}Li	121	2500–4500	ALIBO72B.RTR	Bohlen 1972
^{9}Be(α,α)^{9}Be	136	6000–20000	ABETA65A.RTR	Taylor 1965
^{9}Be(α,α)^{9}Be	157.5	1500–6000	ABEGO73A.RTR	Goss 1973
^{9}Be(α,α)^{9}Be	170.5	575–4200	ABELE94A.RTR	Leavitt 1994
^{10}B(α,α)^{10}B	170.5	975–3275	AB_MC92A.RTR	McIntyre 1992
^{11}B(α,α)^{11}B	150.8	2000–4000	AB_RA72A.RTR	Ramirez 1972
^{11}B(α,α)^{11}B	160.5	4000–8000	AB_OT72A.RTR	Ott 1972
^{11}B(α,α)^{11}B	170.5	980–3300	AB_MC92B.RTR	McIntyre 1992
C(α,α)C	149	4000–12000	AC_MS72A.RTR	Marvin 1972
C(α,α)C	165	1810–9050	AC_FE94A.RTR	Feng 1994
C(α,α)C	167	4000–7500	AC_BI54A.RTR	Bittner 1954
C(α,α)C	170	5000–9000	AC_CH94A.RTR	Cheng 1994
C(α,α)C	170.5	1560–5000	AC_LE89A.RTR	Leavitt 1989
^{13}C(α,α)^{13}C	165	2000–3500	AC_BA65A.RTR	Barnes 1965
^{13}C(α,α)^{13}C	165	3300–6500	AC_KE68A.RTR	Kerr 1968
^{14}N(α,α)^{14}N	163.7	2600–4700	AN_KA58A.RTR	Kashy 1958
^{14}N(α,α)^{14}N	165	2000–6200	AN_FE94A.RTR	Feng 1994
^{14}N(α,α)^{14}N	167	4550–6550	AN_FO93A.RTR	Foster 1993
^{14}N(α,α)^{14}N	167	7090–9070	AN_FO93B.RTR	Foster 1993
^{14}N(α,α)^{14}N	167	8650–9000	AN_FO93C.RTR	Foster 1993
^{14}N(α,α)^{14}N	167.2	2000–4000	AN_HE58A.RTR	Herring 1958
^{15}N(α,α)^{15}N	165.2	1600–2600	AN_SM61A.RTR	Smothich 1961
^{15}N(α,α)^{15}N	165.2	2400–3800	AN_SM61B.RTR	Smothich 1961
^{15}N(α,α)^{15}N	165.2	3800–4800	AN_SM61C.RTR	Smothich 1961
^{15}N(α,α)^{15}N	165.2	4700–5600	AN_SM61D.RTR	Smothich 1961
^{15}N(α,α)^{15}N	165.2	1600–5600	AN_SM61E.RTR	Smothich 1961
^{15}N(α,α)^{15}N	165.2	1600–5600	AN_SM61F.RTR	Smothich 1961
^{15}N(α,α)^{15}N	165.2	3800–4800	AN_MO72A.RTR	Mo 1972
^{16}O(α,α)^{16}O	158.6	6000–10500	AO_HU67A.RTR	Hunt 1967
^{16}O(α,α)^{16}O	165	2050–9000	AO_FE94A.RTR	Feng 1994
^{16}O(α,α)^{16}O	165	9200–9900	AO_CA85A.RTR	Caskey 1985
^{16}O(α,α)^{16}O	165	9600–10500	AO_CA85B.RTR	Caskey 1985

	θ (Lab)	Energy (keV)	File	Reference
$^{16}O(\alpha,\alpha)^{16}O$	165	10320–10700	AO_CA85C.RTR	Caskey 1985
$^{16}O(\alpha,\alpha)^{16}O$	165	10650–11100	AO_CA85D.RTR	Caskey 1985
$^{16}O(\alpha,\alpha)^{16}O$	165	11050–11600	AO_CA85E.RTR	Caskey 1985
$^{16}O(\alpha,\alpha)^{16}O$	165	11500–12500	AO_CA85F.RTR	Caskey 1985
$^{16}O(\alpha,\alpha)^{16}O$	165	12150–12750	AO_CA85G.RTR	Caskey 1985
$^{16}O(\alpha,\alpha)^{16}O$	165	12500–13500	AO_CA85H.RTR	Caskey 1985
$^{16}O(\alpha,\alpha)^{16}O$	165	9150–12750	AO_CA85I.RTR	Caskey 1985
$^{16}O(\alpha,\alpha)^{16}O$	165.7	5000–12500	AO_JO69A.RTR	John 1969
$^{16}O(\alpha,\alpha)^{16}O$	170	2000–9000	AO_CH93A.RTR	Cheng 1993
$^{16}O(\alpha,\alpha)^{16}O$	170	1770–5000	AO_LE90A.RTR	Leavitt 1990
$^{18}O(\alpha,\alpha)^{18}O$	160	2400–3500	AO_PO64A.RTR	Powers 1964
$F(\alpha,\alpha)F$	165	1500–5000	AF_CH93A.RTR	Cheng 1993
$^{19}F(\alpha,\alpha)^{19}F$	170	1500–2300	AF_CS84A.RTR	Cseh 1984
$^{19}F(\alpha,\alpha)^{19}F$	170	2300–3700	AF_CS84B.RTR	Cseh 1984
$^{19}F(\alpha,\alpha)^{19}F$	170	1500–4000	AF_CS84C.RTR	Cseh 1984
$Ne(\alpha,\alpha)Ne$	167.3	2400–3200	ANEGO54A.RTR	Goldberg 1954
$Ne(\alpha,\alpha)Ne$	167.3	3200–4000	ANEGO54B.RTR	Goldberg 1954
$Ne(\alpha,\alpha)Ne$	167.3	2400–4000	ANEGO54C.RTR	Goldberg 1954
$Na(\alpha,\alpha)Na$	165	2000–6000	ANACH91A.RTR	Cheng 1991
$Mg(\alpha,\alpha)Mg$	165	2000–9000	AMGCH93A.RTR	Cheng 1993
$^{24}Mg(\alpha,\alpha)^{24}Mg$	162.5	3150–3900	AMGCS82A.RTR	Cseh 1982
$^{24}Mg(\alpha,\alpha)^{24}Mg$	162.5	4200–4900	AMGCS82B.RTR	Cseh 1982
$^{24}Mg(\alpha,\alpha)^{24}Mg$	164	3150–3900	AMGKA52A.RTR	Kaufmann 1952
$^{24}Mg(\alpha,\alpha)^{24}Mg$	165	5900–6250	AMGIK79A.RTR	Ikossi 1979
$^{24}Mg(\alpha,\alpha)^{24}Mg$	165	6080–6140	AMGIK79B.RTR	Ikossi 1979
$Si(\alpha,\alpha)Si$	170	2000–6000	ASICH93A.RTR	Cheng 1993
$Si(\alpha,\alpha)Si$	170	6000–9000	ASICH93B.RTR	Cheng 1993
$^{28}Si(\alpha,\alpha)^{28}Si$	165	2400–4000	ASILE72A.RTR	Leung 1972
$^{28}Si(\alpha,\alpha)^{28}Si$	165	4000–5000	ASILE72B.RTR	Leung 1972
$^{28}Si(\alpha,\alpha)^{28}Si$	165	5100–6000	ASILE72C.RTR	Leung 1972
$^{28}Si(\alpha,\alpha)^{28}Si$	165	2400–5000	ASILE72D.RTR	Leung 1972
$^{27}Al(\alpha,\alpha)^{27}Al$	170	2000–9000	AALCH93A.RTR	Cheng 1993
$Cl(\alpha,\alpha)Cl$	165	2000–9000	ACLCH93A.RTR	Cheng 1993
$Ar(\alpha,\alpha)Ar$	170	1800–5200	AARLE86A.RTR	Leavitt 1986
$^{39}K(\alpha,\alpha)^{39}K$	175.5	6000–8000	AK_FR82A.RTR	Frekers 1982
$Ca(\alpha,\alpha)Ca$	166	2200–8800	ACAHU90A.RTR	Hubbard 1990
$^{40}Ca(\alpha,\alpha)^{40}Ca$	145	5000–9000	ACASE87A.RTR	Sellschop 1987

Table 3.2: Non-Rutherford ERDA cross-sections.

	θ **(Lab)**	**Energy (keV)**	**File**	**Reference**
H(^{3}He,H)^{3}He	20	2000–3000	1HTP1X1.R33	Terwagne 1996
H(^{3}He,H)^{3}He	30	1900–3000	1HTP1X2.R33	Terwagne 1996
H(α,H)α	10	1000–2500	ERD10H.R33	Quillet 1994
H(α,H)α	20	1000–2500	ERD20H.R33	Quillet 1994
H(α,H)α	30	1000–2500	ERD30H.R33	Quillet 1994
H(α,H)α	30	900–3000	CRSDA.DAT, No. 125	Baglin 1991
H(α,H)α	30	2000–7000	CRSDA.DAT, No. 3	?
D(α,D)α	10	1000–2500	ERD10D.R33	Quillet 1994
D(α,D)α	20	1000–2500	ERD20D.R33	Quillet 1994
D(α,D)α	30	1000–2500	ERD30D.R33	Quillet 1994
D(α,D)α	30	2200–3000	CRSDA.DAT, No. 4	?
D(α,D)α	30	1000–2070	CRSDA.DAT, No. 130	Besenbacher 1986
D(α,D)α	30	2070–2180	CRSDA.DAT, No. 131	Besenbacher 1986
D(α,D)α	30	2180–2800	CRSDA.DAT, No. 132	Besenbacher 1986

Table 3.3: Nuclear reactions cross-sections.

	θ **(Lab)**	**Energy (keV)**	**File**	**Reference**
$D(^3He,\alpha)p$	All	380–1000	CRSDA.DAT, No. 1	?
$D(^3He,\alpha)p$	All	700–2000	CRSDA.DAT, No. 111	?
$D(^3He,\alpha)p$	All	300–2000	CRSDA.DAT, No. 129	?
$D(^3He,p)\alpha$	All	380–1000	CRSDA.DAT, No. 28	?
$^3He(D,\alpha)p$	All	250–660	CRSDA.DAT, No. 2	?
$^3He(D,p)\alpha$	All	250–660	CRSDA.DAT, No. 46	?
$^6Li(p,^3He)^4He$	60	650–2900	6LIP3HE.R33	Marion 1956
$^6Li(p,\alpha)^3He$	60	650–2900	6LIPA.R33	Marion 1956
$^6Li(D,\alpha)^4He$	150	400–1900	6LIDA_1.R33	Maurel 1981
$*^6Li(^3He,p_0)^8Be$	165	900–5100	6LITP0.R33	Schiffer 1956
$*^6Li(^3He,p_1)^8Be$	165	900–5100	6LITP1.R33	Schiffer 1956
$^7Li(p,\alpha)^4He$	150	500–1500	7LIPA.R33	Maurel
$^9Be(D,\alpha_0)^7Li$	165	500–1900	9BEDA0.R33	Biggerstaff 1962
$^9Be(D,\alpha_1)^7Li$	165	500–1600	9BEDA1.R33	Biggerstaff 1962
$^9Be(^3He,p_0)^11B$	90	1800–5100	9BETP0_1.R33	Wolicki
$^9Be(^3He,p_1)^11B$	90	1800–5100	9BETP1_1.R33	Wolicki
$^9Be(^3He,p_0)^11B$	150	1800–5100	9BETP0_2.R33	Wolicki
$^9Be(^3He,p_1)^11B$	150	1800–5100	9BETP1_2.R33	Wolicki
$^{10}B(p,\alpha_0)^7Be$	50	1800–10800	10BPA0_1.R33	Jenkin 1964
$^{10}B(p,\alpha_1)^7Be$	50	2350–10100	10BPA1_1.R33	Jenkin 1964
$^{10}B(p,\alpha_0)^7Be$	90	1800–9500	10BPA0_2.R33	Jenkin 1964
$^{10}B(p,\alpha_1)^7Be$	90	2650–7100	10BPA1_2.R33	Jenkin 1964
$^{10}B(D,\alpha_0)^8Be$	156	980–1800	10BDA0.R33	Purser 1963
$^{10}B(D,\alpha_1)^8Be$	156	980–1800	10BDA1.R33	Purser 1963
$^{10}B(^3He,p_0)^{12}C$	90	1300–5000	10BTP0.R33	Schiffer 1956
$^{10}B(^3He,p_1)^{12}C$	90	1300–5000	10BTP1.R33	Schiffer 1956
$^{10}B(\alpha,p_0)^{13}C$	135	4000–5000	10BAP0.R33	Giorginis 1995
$^{10}B(\alpha,p_1)^{13}C$	135	4000–5000	10BAP1.R33	Giorginis 1995
$^{11}B(^3He,D_0)^{12}C$	90	3000–5400	11BTD0.R33	Holmgren 1959
$^{11}B(^3He,p_0)^{13}C$	90	3000–5400	11BTP0.R33	Holmgren 1959
$^{11}B(^3He,p_{1,2,3})^{13}C$	90	3000–5400	11BTP123.R33	Holmgren 1959
$^{12}C(D,p)^{13}C$	135	520–2950	12CDP_1.R33	Jarjis 1979
$^{12}C(D,p)^{13}C$	165	800–1950	12CDP_2.R33	Kashy 1960
$^{12}C(^3He,p_0)^{14}N$	90	2100–2300	12CTP0.R33	Tong 1990
$^{12}C(^3He,p_1)^{14}N$	90	2100–2400	12CTP1.R33	Tong 1990
$^{12}C(^3He,p_2)^{14}N$	90	2100–2400	12CTP2.R33	Tong 1990
$^{13}C(D,p)^{14}C$	135	600–2950	13CDP.R33	Marion 1956
$^{14}N(D,\alpha_0)^{12}C$	150	600–1400	14NDA0_1.R33	Amsel 1969
$^{14}N(D,\alpha_1)^{12}C$	150	600–1400	14NDA1_1.R33	Amsel 1969
$*^{14}N(D,p_0)^{15}N$	150	500–1900	14NDP0_1.R33	Simpson 1984
$*^{14}N(D,p_{1,2})^{15}N$	150	600–1400	14NDP12.R33	Amsel 1969
$*^{14}N(D,p_3)^{15}N$	150	800–1400	14NDP3.R33	Amsel 1969
$*^{14}N(D,p_{4,5})^{15}N$	150	600–1400	14NDP45.R33	Amsel 1969
$*^{14}N(D,p_5)^{15}N$	150	600–1400	14NDP45.R33	Amsel 1969
$^{14}N(^3He,p_{1,2})^{16}O$	90	1600–2800	14NTP1X1.R33	Terwagne 1994
$^{14}N(^3He,p_{1,2})^{16}O$	135	1600–2800	14NTP1X2.R33	Terwagne 1994
$^{14}N(^3He,p_3)^{16}O$	90	1600–2800	14NTP3X1.R33	Terwagne 1994
$^{14}N(^3He,p_3)^{16}O$	135	1600–2800	14NTP3X2.R33	Terwagne 1994
$^{14}N(^3He,p_4)^{16}O$	90	1600–2800	14NTP4X1.R33	Terwagne 1994
$^{14}N(^3He,p_4)^{16}O$	135	1600–2800	14NTP4X2.R33	Terwagne 1994
$^{14}N(^3He,p_5)^{16}O$	90	1600–2800	14NTP5X1.R33	Terwagne 1994
$^{14}N(^3He,p_5)^{16}O$	135	1600–2800	14NTP5X2.R33	Terwagne 1994

	θ (Lab)	Energy (keV)	File	Reference
^{14}N(^{3}He,p$_7$)^{16}O	90	1600–2800	14NTP7X1.R33	Terwagne 1994
^{14}N(^{3}He,p$_7$)^{16}O	135	1600–2800	14NTP7X2.R33	Terwagne 1994
^{14}N(^{3}He,α_0)^{13}N	90	1600–2800	14NTA0X1.R33	Terwagne 1994
^{14}N(^{3}He,α_0)^{13}N	135	1600–2800	14NTA0X2.R33	Terwagne 1994
^{14}N(α,p$_0$)^{17}O	135	4000–5000	14NAP1.R33	Giorginis 1995
$*^{15}$N(p,α)^{12}C	140	900–2860	15NPA.R33	Hagedorn 1957
^{15}N(D,α)^{13}C	150	800–1300	15NDA_1.R33	Sawicki 1985
^{16}O(D,α)^{14}N	135	800–2000	16ODA_2.R33	Amsel 1964
^{16}O(D,α)^{14}N	145	760–950	16ODA_1.R33	Turos 1973
^{16}O(D,α)^{14}N	165	800–2000	16ODA_3.R33	Amsel 1964
^{16}O(D,p$_0$)^{17}O	135	20–3000	16ODP0_1.R33	Jarjis 1979
^{16}O(D,p$_1$)^{17}O	135	500–3000	16ODP1_2.R33	Jarjis 1979
^{16}O(D,p$_1$)^{17}O	155	400–1100	16ODP1_1.R33	Amsel 1967
^{16}O(^{3}He,α)^{15}O	90	1600–2600	16OTA.R33	Abel
$*^{18}$O(p,α)^{15}N	155	1500–1800	18OPA_2.R33	Alkemada
$*^{18}$O(p,α)^{15}N	165	500–1000	18OPA_1.R33	Amsel 1967
^{18}O(D,α_0)^{16}N	165	830–2000	18ODA_1.R33	Amsel 1964
^{18}O(D,α_1)^{16}N	165	830–2000	18ODA_2.R33	Amsel 1964
^{18}O(D,α_2)^{16}N	165	830–2000	18ODA_3.R33	Amsel 1964
^{18}O(D,α_3)^{16}N	165	830–2000	18ODA_4.R33	Amsel 1964
$*^{19}$F(p,α)^{16}O	90	700–1900	19FPA_1.R33	Dieumegard 1980
$*^{19}$F(p,α)^{16}O	150	700–2000	19FPA_2.R33	Dieumegard 1980
^{19}F(D,α_0)^{17}O	150	700–1900	19FDA0_1.R33	Maurel 1981
^{19}F(D,α_1)^{17}O	150	1000–1900	19FDA1_1.R33	Maurel 1981

3.7 The `Calculate` menu

In the `Calculate` menu all commands for calculating spectra, scattering kinematics, stopping powers and data fitting are located.

- `Calculate Spectrum`: Calculates the simulated spectrum.
- `Calculate Spectrum Fast`: Sets the detector resolution to 0.0 keV, ignores straggling and dual scattering and calculates the simulated spectrum. The calculation of the spectrum is performed much faster than with `Calculate Spectrum`, but the spectrum will contain kinks.
- `Fit Spectrum...`: Data fitting to experimental data. See section 3.7.1 for details.
- `Kinematics...`: Calculation of scattering kinematics. Allows the calculation of the energies of backscattered particles, recoils and nuclear reaction products.
- `Stopping...`: Calculation of stopping powers for any projectile in any target element and of energy loss in the different layers.

  Note: The result of a stopping power calculation for $E > 1$ MeV/amu depends on the setting of `Setup Calculation:High energy stopping`, see section 3.4.2.

3.7.1 `Fit Spectrum...`

Data fitting to backscattering spectra is a nontrivial task. In data fitting the quadratic deviation of the simulated from the measured data points

$$\chi^2 = \sum_i w(i)\ (N_{exp}(i) - N_{sim}(i))^2 \tag{3.2}$$

is minimised by varying the input parameters of the calculation. $N_{exp}(i)$ is the number of counts in channel i of the measured spectrum, and $N_{sim}(i)$ is the number of counts in channel i of the simulated spectrum. $w(i)$ is the weight of each data point.

Fast fitting algorithms, such as the Levenberg-Marquardt algorithm, tend to be unstable and require the knowledge of the derivatives of χ^2. SIMNRA uses the Simplex algorithm for fitting [2]. The Simplex algorithm is very stable and converges (nearly) always. However, the convergence is not very fast. The Simplex algorithm always uses $n + 1$ points (called vertices) in the parameter space for fitting, where n is the number of free parameters.

SIMNRA uses equal weighting of each data point, this means $w(i) = 1$ for all points.

You can fit:

1. Energy calibration
2. Particles*sr
3. Thickness of a layer
4. Composition of a layer

independently or all at once. Check which parameters should be varied. Only one layer at a time can be fitted.

- `Fitting range`: The range (in channels) in which χ^2 is calculated.
- `Max Iterations`: The maximum number of iterations. Fitting will be performed until the desired accuracy is reached or the maximum number of iterations is reached.
- `Max Error`: The desired accuracy of the fit. The fit has converged if the relative change of all fitted parameters and of χ^2 is below `Max Error`. The relative change of a parameter A is $\Delta A/A$, where ΔA is the difference between the best vertex (the vertex with the lowest χ^2) and the worst vertex (the vertex with the highest χ^2).
- `fast` and `accurate` fit: If `fast` fit is selected, the fit will be performed with zero detector resolution and without calculation of straggling and dual scattering, see `Calculate Spectrum Fast`. This will speed up the fit significantly, but is less accurate.

  If `accurate` fit is selected, the actual detector resolution, straggling (if checked in the `Setup:Calculation` menu) and dual scattering (if checked in the `Setup:Calculation` menu) are used for the calculation.

3.8 The `Plot` menu

This section describes all plot related commands, including all commands which are not accessible via menus.

- `Autoscaling`: If checked, the plot will be scaled automatically to minimum and maximum if experimental data are imported or a new calculation is performed. If unchecked, the axis scales remain fixed.
- `Delete experimental data`: Deletes the experimental data from the plot.
- `Delete simulated data`: Deletes all simulated data from the plot.
- **Scaling the axis:** To scale the x- or y-axis double-click with the left mouse button on the desired axis. Enter the axis minimum and maximum.
- **Zooming into the plot:** To zoom into the plot click with the left mouse button into the upper left corner of the range you want to zoom in. Keep the mouse button down and tear a rectangle to the lower right corner of the zooming range. Release the left mouse button. Now double-click with the left mouse button into the rectangle to zoom in.
- **Zooming out:** Click the right mouse button to zoom out.

3.9 The `Options` menu

- `Directories`: Directories where atomic data (file ATOMDATA.DAT), stopping data (the files STOPH.DAT and STOPHE.DAT) and cross-section data are located.

- `Create Reaction List`: SIMNRA uses a file named CRSEC.LST in the cross-sections directory to know which cross-section data are available. `Create Reaction List` will create this file. You have to recreate the reaction list if you add or delete cross-section data files.

  Note: Some data files contain total cross-sections. These files are ignored by SIMNRA. The program displays a list of all ignored files.

3.10 Adding new cross-section data

To add new cross-section data, you have to perform the following steps:

1. Create a cross-section data file in the R33 file format. The file format is described below.

2. Copy this file into the directory where all other cross-section data files are. This directory is displayed in `Options:Directories...`.

3. Recreate the reaction list by clicking `Options:Create Reaction List`.

   Note: If your file will be ignored, then SIMNRA was not able to read or understand the file. Carefully read the section about the R33 file format and try again.

3.10.1 The R33 file format

The R33 file format is described in full detail in a proposal by I.C. Vickridge. The proposal can be obtained from SigmaBase. An example for a valid file in the R33 format is shown in fig. 3.5. Each line must end with <CR><LF> (Carriage Return and Line Feed).

SIMNRA uses not only the data points, but also a part of the information supplied in the file header. The following lines must be present in the file in the given order. The file may additionally contain an arbitrary number of other information. All other lines than the ones listed below are ignored by the program.

- A line containing the string 'REACTION:'. Uppercase characters are important. SIMNRA will interpret the nuclear reaction string written in that line (In the example of fig. 3.5 16O(d,a0)14N) to find out which particles are involved in the nuclear reaction. The masses of the particles are ignored.

- A line containing the string 'MASSES:'. SIMNRA will read the masses of the particles from this line. Please note that the first mass is the mass of the incident particle, the second mass is the mass of the target particle, the third mass is the mass of the outgoing particle for which the cross-section is valid and the fourth mass is the mass of the other reaction product.

- A line containing the string 'QVALUE:'. The Q-value is the energy released in the nuclear reaction (in keV).

```
COMMENT: These cross sections have been digitised from the publication
cited below.  No error of either the energy and or the sigma is given.
Some errors may be among the data, we are recently checking them.
The Los Alamos Ion Beam Handbook also will contain these data as soon
as it is ready.  If you use this data please refer to the paper below.
Source:  A.Turos, L.Wielunski and a Batcz, NIM, 111(1973), 605
Special comment:
WARNING ! THIS IS MAINLY FOR TEST NO GUARANTY IS PROVIDED FOR EVEN
AGREEMENT WITH THE ORIGINAL PUBLICATION.

NAME: Gyorgy Vizkelethy
ADDRESS1:  Department of Physics
ADDRESS2:  Idaho State University
ADDRESS3:  Campus Box 8106
ADDRESS4:  Pocatello, ID 83209-8106
ADDRESS5:  (208) 236-2626
ADDRESS6:  vizkel@physics.isu.edu
SERIAL NUMBER: ?
REACTION: 16O(d,a0)14N
DISTRIBUTION: Energy
MASSES: 2,16,4,14
QVALUE: 3110.00
THETA: 145.0
SIGFACTORS: 1.00 0.00
ENFACTORS 1.00 0.00 0.00 0.00
NVALUES: 5
761.0     0.0     2.92E+0000     0.0
770.0     0.0     3.65E+0000     0.0
775.0     0.0     3.99E+0000     0.0
780.0     0.0     4.41E+0000     0.0
785.0     0.0     4.55E+0000     0.0
```

Figure 3.5: Example for a cross-section data file in the R33 file format.

- A line containing the string 'THETA:'. Theta should be given in degrees. The value of theta is not used by SIMNRA, however this line must be present and contain a value.
- A line containing the string 'NVALUES:'. The value of nvalues is ignored, however this line must be present. SIMNRA assumes that the data will start after this line.
- The data are organised in 4 columns: The first column is the energy in keV, the second column is the energy error (ignored by SIMNRA), the third column is the differential cross-section in the laboratory frame measured in mbarn/sr, and the fourth column is the cross-section error (ignored by SIMNRA). SIMNRA expects the data to be arranged in order of ascending energy.

3.11 Detector nonlinearity

It is well known that the energy calibration of semiconductor detectors, which are used in most ion beam experiments, is not exactly linear. This is due to the energy dependent energy loss in the top electrode and the dead layer of the semiconductor detector [3, 4], which results in a nonlinearity of typically several channels.

To account for detector nonlinearities, SIMNRA offers two possibilities:

1. You can create a foil consisting of two layers in front of the detector. Layer 2 is composed of the material of the top electrode (usually Au) and has the thickness of the electrode (usually the thickness is supplied by the manufacturer of the detector). Layer 1 is composed of silicon in the case of a silicon detector and has the thickness of the dead layer (the dead layer is the insensitive region near the electrode). The dead layer thickness can be obtained only experimentally by tilting the detector.

2. SIMNRA offers the possibility to use a non-linear energy calibration with a quadratic correction term of the form

$$E\,[\mathrm{keV}] = A + B \times \mathrm{channel} + C \times \mathrm{channel}^2.$$

   See section 3.4.1 for details.

Chapter 4

Physics

4.1 Overview

During the last decade, several programs for the simulation of backscattering spectra have been developed. The most common program is Doolittle's RUMP [5, 6]. However, RUMP uses many approximations to save computing time. The increase in computer power during the last years has made it possible to drop several of the approximations used by RUMP. SIMNRA offers more freedom in the use of non-Rutherford cross-sections and nuclear reactions, treats several topics such as straggling and convolution more precise and adds new possibilities such as dual scattering. This section describes the physics involved in the simulation of a backscattering spectrum as performed by SIMNRA.

The target is subdivided into shallow sublayers. Each simulated spectrum is made up of the superimposed contributions from each isotope of each sublayer of the sample target. The thickness of each sublayer is chosen in such a way that the energy loss in each sublayer is about the stepwidth of the incoming particles. When the incident particles penetrate a sublayer, they loose energy due to electronic and nuclear energy loss and the beam energy is spread due to straggling. The calculation of the energy loss is described in detail in section 4.3, and the calculation of straggling in section 4.5. SIMNRA calculates the energy of backscattered particles[1] from the front and the backside of the sublayer, and the energy of these particles when reaching the detector after passing to the target surface and traversing a foil in front of the detector, see fig. 4.1. The contribution of each isotope in each sublayer will be referred to as a brick.

[1] A 'backscattered' particle may be a recoil or a product in a nuclear reaction as well.

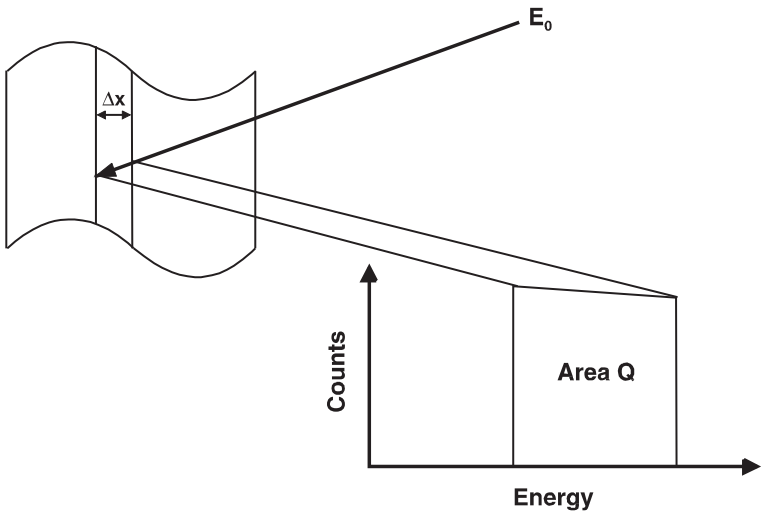

Figure 4.1: Notation used for a single brick.

To account for energy straggling and the finite energy resolution of the detector the brick shown in fig. 4.1 is convoluted with a Gaussian function $f(E, \sigma^2)$ with width

$$\sigma^2 = \sigma^2_{\text{Straggling Out}} + \sigma^2_{\text{Detector}}. \tag{4.1}$$

$\sigma^2_{\text{Straggling Out}}$ is the variance of the energy distribution of the outgoing particles due to energy loss straggling, and $\sigma^2_{\text{Detector}}$ is the energy resolution of the detector.

The final contribution to the energy spectrum of each isotope in each sublayer is given by

$$S(E) = \int_0^\infty S_0(E')\, f(E', \sigma^2(E'))\, dE' \tag{4.2}$$

Here $S_0(E)$ is the energy spectrum before convolution and $S(E)$ the spectrum after the convolution. Note that the width of the Gaussian changes throughout the brick due to different straggling contributions.

The Number of counts N_i in each channel i is given by integrating $S(E)$ over the channel width from the minimum to the maximum energy of each channel:

$$N_i = \int_{E_{min}(i)}^{E_{max}(i)} S(E')\, dE' \tag{4.3}$$

Eqs. 4.2 and 4.3 can be put together into a 2-dimensional integral, which is computed by SIMNRA by means of a 2-dimensional Gauss-Legendre integration. The accuracy of the integration is about 10^{-4}.

The area Q of the brick in fig. 4.1 is calculated by SIMNRA by using the cross-section

at the mean energy $\bar{E}$ in the brick.

$$Q = N\Delta\Omega \frac{d\sigma}{d\Omega}(\bar{E}) \frac{\Delta x}{\cos\alpha} \tag{4.4}$$

$N\Delta\Omega$ is the number of incident particles times the solid angle of the detector and $d\sigma/d\Omega(\bar{E})$ is the differential cross-section evaluated at the mean energy $\bar{E}$. The heights of the front and back side of the brick are adjusted to give the correct area when integrated. SIMNRA interpolates the brick linearly, as shown in fig. 4.1. This is, however, only valid if the cross-section does not vary strongly and the brick is sufficiently thin. If the cross-section has structures such as sharp resonances, the stepwidth of the incoming particles must be sufficiently smaller than the width of the resonance.

4.2 Cross-sections

4.2.1 Rutherford cross-sections

The Rutherford cross-section for backscattering is given in the laboratory system by

$$\sigma_R\ [\mathrm{mb/sr}] = 5.18275 \times 10^6 \left(\frac{Z_1 Z_2}{E\ [\mathrm{keV}]}\right)^2 \frac{\left\{\left(M_2^2 - M_1^2 \sin^2\theta\right)^{1/2} + M_2 \cos\theta\right\}^2}{M_2 \sin^4\theta\ \left(M_2^2 - M_1^2 \sin^2\theta\right)^{1/2}} \tag{4.5}$$

θ is the scattering angle, Z_1 and M_1 are the nuclear charge and the mass of the projectile, respectively, and Z_2 and M_2 are the nuclear charge and the mass of the target atom, respectively. σ_R is the differential cross-section in the laboratory system. Experimental measurements indicate that actual cross-sections deviate from Rutherford at both high and low energies for all projectile-target pairs. The low-energy departures are caused by partial screening of the nuclear charges by the electron shells surrounding both nuclei [7, 8, 9, 1]. This screening is taken into account by a correction factor F:

$$\sigma = F\sigma_R$$

For $\theta > 90°$ the correction factor by L'Ecuyer *et al.* [7] is widely used:

$$F_{\mathrm{L'Ecuyer}} = 1 - \frac{0.049\, Z_1 Z_2^{4/3}}{E_{CM}} \tag{4.6}$$

E_{CM} is the energy in the center of mass system (in keV). Tabulated values of $F_{\mathrm{L'Ecuyer}}$ can be found for example in [1]. The correction for backscattering angles $\theta > 90°$ at

typical energies used in ion beam analysis usually is small. For 1 MeV ^{4}He ions on gold the correction is only about 3.5%.

The correction factor by L'Ecuyer (eq. 4.6) is a first order correction and does not take into account the influence of the scattering angle θ. For $\theta < 90°$ eq. 4.6 will underestimate the necessary correction to the Rutherford cross-section. SIMNRA uses the angular- and energy dependent correction factor by Andersen *et al.* [9]:

$$F_{\text{Andersen}} = \frac{\left(1 + \frac{1}{2}\frac{V_1}{E_{CM}}\right)^2}{\left\{1 + \frac{V_1}{E_{CM}} + \left[\frac{V_1}{2E_{CM}\sin\theta_{CM}/2}\right]^2\right\}^2} \tag{4.7}$$

θ_{CM} is the scattering angle in the center of mass system. The increase in the kinetic energy V_1 is given by

$$V_1\ [\text{keV}] = 0.04873\, Z_1 Z_2 \left(Z_1^{2/3} + Z_2^{2/3}\right)^{1/2}$$

The dependence of the correction factor F_{Andersen} from the scattering angle θ for ^{4}He scattered from gold is shown in fig. 4.2 for different ^{4}He energies. Dashed lines are the angular independent correction factor by L'Ecuyer. For large scattering angles the correction factors by L'Ecuyer and Andersen are near to unity and similar, however, for small scattering angles the correction by Andersen becomes large and the angle-independent L'Ecuyer correction underestimates the deviations from the Rutherford cross-section.

The Rutherford cross-section for recoils is given in the laboratory system by

$$\sigma_R^{ERD}\ [\text{mb/sr}] = 2.0731 \times 10^7 \frac{[Z_1 Z_2 (M_1 + M_2)]^2}{(2M_2 E\ [\text{keV}])^2 \cos^3\theta} \tag{4.8}$$

θ is the recoil angle in the lab system. SIMNRA applies the correction to the Rutherford cross-section from eq. 4.7 also for the recoil cross-section.

4.2.2 Non-Rutherford cross-sections

At high energies the cross-sections deviate from Rutherford due to the influence of the nuclear force. A useful formula above which energy E_{NR} deviations from Rutherford can be expected was given by Bozoian [10, 11, 12]:

$$\begin{aligned} E_{NR}\ [\text{MeV}] &= \frac{M_1 + M_2}{M_2}\frac{Z_2}{10} \quad \text{for } Z_1 = 1 \\ E_{NR}\ [\text{MeV}] &= \frac{M_1 + M_2}{M_2}\frac{Z_1 Z_2}{8} \quad \text{for } Z_1 > 1 \end{aligned}$$

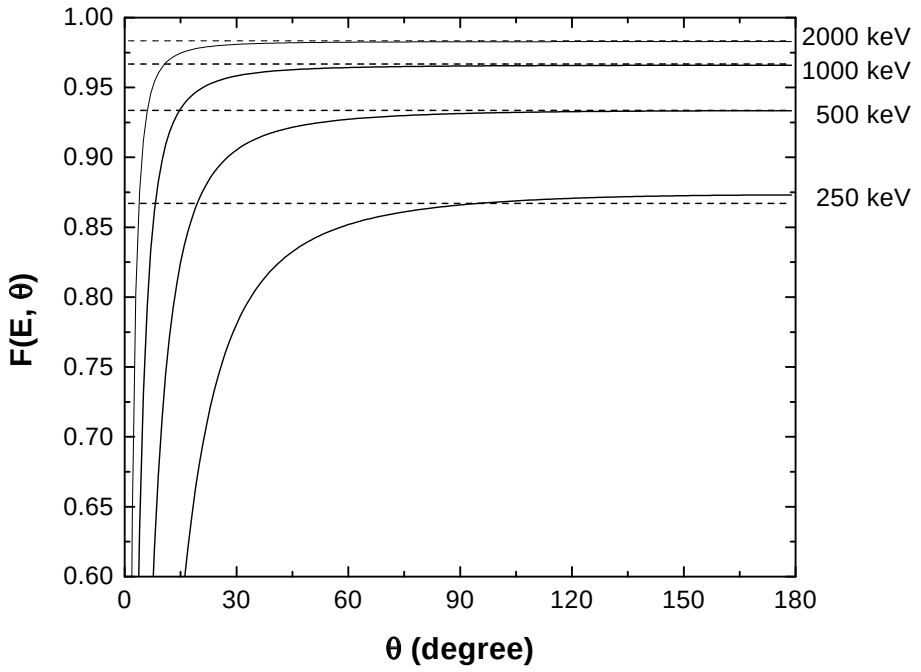

Figure 4.2: Angular dependence of the correction factors for the Rutherford cross-section by L'Ecuyer (eq. 4.6, dashed lines) and Andersen (eq. 4.7, solid lines) for ^{4}He backscattered from gold at different energies.

E_{NR} is the energy at which the deviation from the Rutherford cross-section is $> 4\%$.

SIMNRA does not check if the cross-sections at a given energy are Rutherford or not. It is in the responsibility of the user to choose the correct cross-sections. The above formulas may be useful to estimate if the cross-section is still Rutherford or not.

For non-Rutherford cross-sections SIMNRA uses experimentally determined differential cross-sections taken from SigmaBase. The use of non-Rutherford cross-sections is described in full detail in section 3.6. SIMNRA uses linear interpolation between the given data points.

4.3 Evaluation of energy loss

The energy E of a particle in the depth x is given by the integral equation

$$E(x) = E_0 - \int_0^{x/\cos\alpha} \frac{dE}{dx'}(E(x'), x')dx' \tag{4.9}$$

Here we assume that the particle starts with initial energy E_0 at the surface ($x = 0$), $dE/dx'(E(x'), x')$ is the energy and depth dependent stopping power. In principle, eq. 4.9

can be evaluated directly, however this consumes a lot of computing time.

For the evaluation of the energy loss SIMNRA uses the algorithm of Doolittle instead, developed for RUMP [5]. The beam loses energy according to the differential equation

$$\frac{dE}{dx} = -\epsilon(E) \tag{4.10}$$

where this is the defining equation for $\epsilon(E)$, the energy dependent stopping cross-section. x is the pathlength into the material, measured in areal density (10^{15} atoms/cm^2). SIMNRA uses the Ziegler stopping power data, see section 4.4. $\epsilon' = d\epsilon/dE$ is the first and $\epsilon'' = d^2\epsilon/dE^2$ the second derivative of ϵ.

If incoming or outgoing particles with incident energy E_0 traverse a layer of material with thickness Δx, then the particles energy E_1 after the layer can be expanded into a Taylor series:

$$E_1 = E_0 + \Delta x \frac{dE}{dx}(E_0) + \frac{1}{2}\Delta x^2 \frac{d^2E}{dx^2}(E_0) + \frac{1}{6}\Delta x^3 \frac{d^3E}{dx^3}(E_0) \tag{4.11}$$

The terms in eq. 4.11 look as follows:

$$\frac{dE}{dx} = -\epsilon \tag{4.12}$$

$$\frac{d^2E}{dx^2} = \frac{d}{dx}(-\epsilon) = -\frac{d\epsilon}{dE}\frac{dE}{dx} = \epsilon'\epsilon \tag{4.13}$$

$$\frac{d^3E}{dx^3} = \frac{d}{dx}(\epsilon'\epsilon) = \frac{d\epsilon'}{dx}\epsilon + \epsilon'\frac{d\epsilon}{dx} = -\epsilon''\epsilon^2 - \epsilon'^2\epsilon \tag{4.14}$$

With ϵ, ϵ' and ϵ'' evaluated at E_0

$$E_1 = E_0 - \Delta x\epsilon + \frac{1}{2}\Delta x^2\epsilon\epsilon' - \frac{1}{6}\Delta x^3\left(\epsilon''\epsilon^2 + \epsilon'^2\epsilon\right) \tag{4.15}$$

See ref. [5] for a discussion of the accuracy of the above equations.

ϵ' and ϵ'' are calculated by SIMNRA by numerical differentiation of the Ziegler stopping power data. The stepwidth Δx for the incoming and outgoing particles can be adjusted in the `Setup:Calculation` menu. The stepwidth of the incoming particle should be kept small in the range of 10 keV due to the cross-section calculation, see section 4.1. The stepwidth for outgoing particles can be chosen much larger due to the accuracy of eq. 4.15. Typical values for the stepwidth of outgoing particles are around 200 keV.

4.4 Stopping power data

4.4.1 Hydrogen

SIMNRA uses the electronic stopping power data by Andersen and Ziegler [13] for the stopping of incident protons, deuterons and tritons in all elements. The electronic stopping power S_e in eV/(10^{15} atoms/cm^2) for an incident hydrogen ion with energy/mass E in keV/amu is given by

$$\frac{1}{S_e} = \frac{1}{S_{Low}} + \frac{1}{S_{High}} \tag{4.16}$$

with

$$S_{Low} = A_2\, E^{0.45} \tag{4.17}$$

and

$$S_{High} = \frac{A_3}{E} \ln\left[1 + \frac{A_4}{E} + A_5 E\right] \tag{4.18}$$

$A_2 - A_5$ are fitting coefficients and tabulated in [13]. They are stored in the file STOPH.DAT. Equations 4.16–4.18 are valid for 10 keV $\leq E <$ 1 MeV. For energies in the range 1 MeV–100 MeV the electronic stopping power S_e is given by

$$S_e = \frac{A_6}{\beta^2}\left[\ln\frac{A_7\beta^2}{1-\beta^2} - \beta^2 - \sum_{i=0}^{4} A_{i+8}\,(\ln E)^i\right] \tag{4.19}$$

$A_6 - A_{12}$ are tabulated in [13], $\beta = v/c$, with v the ion velocity and c the speed of light. Equation 4.19 is used only if the switch `High energy stopping` in the `Setup:Calculation` menu is checked. If unchecked, the program will use Equations 4.16–4.18 at all energies. The program default is checked. The difference between eq. 4.16 and eq. 4.19 is small in most cases. The main problem using eq. 4.19 is that the first and second derivatives of eq. 4.16 and eq. 4.19 do not fit smoothly together at 1 MeV/amu. This may result in the appearance of kinks in the spectrum.

Nuclear stopping for incident hydrogen, deuterium and tritium ions is negligible for incident energies above about 10 keV/amu [13] and is neglected by SIMNRA.

4.4.2 Helium

For incident ^{3}He and ^{4}He ions the electronic stopping power data by Ziegler [14] are used for all elements. The electronic stopping power S_e in eV/(10^{15} atoms/cm^2) for incident

^{4}He ions with energy E in keV is given by

$$\frac{1}{S_e} = \frac{1}{S_{Low}} + \frac{1}{S_{High}} \tag{4.20}$$

with

$$S_{Low} = A_1 \, E^{A_2} \tag{4.21}$$

and

$$S_{High} = \frac{A_3}{E} \ln\left[1 + \frac{A_4}{E} + A_5 E\right] \tag{4.22}$$

$A_1 - A_5$ are fitting coefficients and tabulated in [14]. They are stored in the file STOPHE.DAT. Equations 4.20–4.22 are valid for 1 keV $\leq E <$ 10 MeV. ^{4}He-stopping at higher energies (above 10 MeV) is not implemented in the program.

The stopping power of ^{3}He is identical to the stopping power of ^{4}He at the same velocity [14]. The stopping power of ^{3}He with energy E is obtained by taking the stopping power value at the energy $E(^4\text{He}) = 4/3\, E(^3\text{He})$. The stopping power for ^{3}He is valid in the energy range 10 keV $\leq E <$ 7.5 MeV.

Nuclear stopping for incident helium ions is calculated with the Krypton-Carbon (Kr-C) potential [15]. The nuclear stopping S_n in eV/10^{15} atoms/cm^2 for He-ions with incident energy E (in keV) is given by:

$$S_n = s_n \frac{8.462\, Z_1\, Z_2\, M_1}{(M_1 + M_2)\left(Z_1^{2/3} + Z_2^{2/3}\right)^{1/2}} \tag{4.23}$$

s_n is the reduced nuclear stopping and Z_1, M_1 are the nuclear charge and mass of the helium ion and Z_2, M_2 are the nuclear charge and mass of the target element. The reduced nuclear stopping s_n has the simple form

$$s_n = 0.5 \, \frac{\ln(1+\epsilon)}{\epsilon + 0.10718\, \epsilon^{0.37544}} \tag{4.24}$$

ϵ is the reduced energy and is given by

$$\epsilon = \frac{32.53\, M_2\, E}{Z_1 Z_2\, (M_1 + M_2)\left(Z_1^{2/3} + Z_2^{2/3}\right)^{1/2}} \tag{4.25}$$

Nuclear stopping is only important at incident energies $E <$ 100 keV, at higher energies nuclear stopping becomes negligible.

4.4.3 Heavy ions

The electronic stopping power of heavy ions in all elements is derived from the stopping power of protons using Brandt-Kitagawa theory [16]. The formalism is described in detail in ref. [16]. The screening length Λ (eq. 3-29 of ref. [16]) is multiplied by an empirical correction factor which has been digitised from fig. 3-25 of ref. [16]. The correction factor for all elements is stored in the file LCORRHI.DAT.

Note that the switch `High energy stopping` in the `Setup:Calculation` menu has influence on the calculation of the stopping power for heavy ions with incident energies above 1 MeV/amu.

Nuclear stopping for incident heavy ions is calculated with the universal potential from ref. [16]. The reduced nuclear stopping s_n with the universal potential is given by

$$s_n = \frac{\ln(1 + 1.1383\,\epsilon)}{2\,[\epsilon + 0.01321\,\epsilon^{0.21226} + 0.19593\,\epsilon^{0.5}]} \tag{4.26}$$

for $\epsilon \leq 30$. For $\epsilon > 30$ s_n is given by

$$s_n = \frac{\ln(\epsilon)}{2\epsilon} \tag{4.27}$$

The reduced energy ϵ in eqs. 4.26 and 4.27 is calculated using the universal screening length a_U, which is $\propto 1/(Z_1^{0.23} + Z_2^{0.23})$ instead of the Firsov screening length $a_F \propto 1/(Z_1^{2/3} + Z_2^{2/3})^{1/2}$, which is used in eq. 4.25. The difference between eq. 4.24 and 4.26 is only some percent.

The nuclear stopping component is only important at ion energies below about 200 keV/amu. Nuclear stopping becomes very small at higher energies, typically below 1% of the electronic stopping component.

4.4.4 Stopping in compounds

SIMNRA uses Bragg's rule [17] for the determination of the stopping power in compounds. Bragg's rule is a simple linear additivity rule of the stopping contributions of the different compound elements, assuming that the interaction of an incident ion with a target atom is independent of the surrounding target atoms. For a compound consisting of different elements i with atomic concentrations c_i ($\sum c_i = 1$) the total stopping power S is given by

$$S = \sum c_i\, S_i \tag{4.28}$$

S_i is the stopping power of each element.

Bragg's rule assumes that the interaction between the ion and the atom is independent of the environment. The chemical and physical state of the medium is, however, observed to have an effect on the energy loss. The deviations from Bragg's rule predictions are most pronounced around the stopping power maximum and for solid compounds containing heavier constituents, such as oxides, nitrides, hydrocarbons, etc. The deviations from Bragg's rule predictions may be of the order of 10–20% [18].

Ziegler and Manoyan [19] have developed the 'cores and bonds' (CAB) model, which assumes the electronic energy loss to have two contributions: The effect of the cores and the effect of the bonds, such as C-H and C-C. The CAB-model allows better predictions for the stopping in compounds, however, the bond structure has to be known. Currently the CAB-model (or any other model which allows better predictions for the stopping in compounds) is not implemented in SIMNRA.

4.5 Straggling

When a beam of charged particles penetrates matter, the slowing down is accompanied by a spread in the beam energy. This phenomenon is called straggling. It is due to statistical fluctuations of the energy transfer in the collision processes.

Energy loss straggling has different contributions:

1. Electronic energy loss straggling due to statistical fluctuations in the transfer of energy to electrons.

2. Nuclear energy loss straggling due to statistical fluctuations in the nuclear energy loss. Though the contribution of the nuclear energy loss to the total energy loss is usually negligible at high energies, it contributes to the total energy loss straggling. The contribution of the nuclear energy loss straggling is, however, always smaller than the contribution of the electronic energy loss straggling.

3. Straggling due to plural scattering and multiple small angle scattering, resulting in different path lengths and energy and angular spread of the incident beam.

4. Geometrical straggling due to finite detector solid angle and finite beam spot size, resulting in a distribution of scattering angles and different pathlengths for outgoing

particles.

5. Straggling due to surface and interlayer roughness.

An additional contribution to the energy broadening visible in experimental spectra is the energy resolution of the detector. The different straggling contributions have been recently reviewed by Szilágy *et. al.* [20].

Multiple small angle scattering, geometrical straggling and surface roughness are not calculated by SIMNRA. The finite energy resolution of the detector is included in the calculations. Plural scattering with two scattering events (= dual scattering) can be calculated by SIMNRA.

4.5.1 Electronic and nuclear energy loss straggling

There are four main theories describing electronic and nuclear energy loss straggling [21, 22, 23], each applicable in a different regime of energy loss. With ΔE the mean energy loss of the beam, and E the energy of the incident beam, we can distinguish:

$\Delta E/E < 10\%$	**Vavilov's Theory**[24, 22]. For thin layers and small energy losses. The energy distribution is non-Gaussian and asymmetrical. This energy range is not described properly by SIMNRA.
$10 - 20\%$	**Bohr's Theory**[25, 26]. As the number of collisions becomes large, the distribution of particle energies becomes Gaussian.
$20 - 50\%$	**Symon's Theory**[21]. This theory includes non-statistical broadening caused by the change in stopping power over the particle energy distribution. If the mean energy of the beam is higher than the energy of the stopping power maximum, then particles with a lower energy have a higher stopping power, and particles with higher energy have a smaller stopping power. This results in a nonstatistical broadening of the energy distribution. The width of the particles energy distribution in Symon's theory is significantly higher than predicted by Bohr's theory. The distribution of particle energies is still Gaussian.
$50 - 90\%$	**Payne's and Tschalärs Theory** [27, 28, 29]. When the energy losses become very large and the mean energy of the beam decreases below the energy of the stopping power maximum, the particle energy distribution again become skewed, because now particles with lower energy have a lower stopping power than particles with higher energy. The distribution is about Gaussian.

SIMNRA always assumes that the particles energy distribution is Gaussian. This is only an approximation for thin layers: In this case the energy distribution is described by the Vavilov distribution [24, 22]. However, the straggling contribution of thin layers to the total energy broadening is much smaller than the contribution of the finite energy resolution of the detector.

SIMNRA calculates the non-statistic broadening (or skewing) of the energy distribution in the following way:

Assume two particles with energies E_1 and E_2

$$\begin{aligned} E_1 &= E_0 + \frac{\Delta E}{2} \\ E_2 &= E_0 - \frac{\Delta E}{2} \end{aligned}$$

centered around a mean energy E_0. The energy difference $E_1 - E_2$ of the two particles is ΔE. To evaluate the stopping power $\epsilon = dE/dx$ at E_1 and E_2 we can apply a Taylor expansion of the stopping power $\epsilon(E)$ and considering only the linear term:

$$\begin{aligned} \epsilon(E_1) &= \epsilon(E_0) + \frac{1}{2}\frac{d\epsilon}{dE}(E_0)\Delta E \\ \epsilon(E_2) &= \epsilon(E_0) - \frac{1}{2}\frac{d\epsilon}{dE}(E_0)\Delta E. \end{aligned}$$

The energies E_1' and E_2' after penetrating a thin layer with thickness Δx are then given by

$$\begin{aligned} E_1' &= E_1 - \epsilon(E_1)\Delta x \\ E_2' &= E_2 - \epsilon(E_2)\Delta x. \end{aligned}$$

By putting the above equations together we get the energy difference $\Delta E' = E_1' - E_2'$ of the two particles after penetrating the layer:

$$\Delta E' = \left(1 - \frac{d\epsilon}{dE}(E_0)\Delta x\right)\Delta E. \tag{4.29}$$

If $d\epsilon/dE$ is negative, which is the case for all energies above the stopping power maximum, the energy difference increases and the distribution function is broadened. If $d\epsilon/dE$ is positive, the energy difference decreases and the distribution function gets skewed. Because this is a linear Taylor expansion, a Gaussian distribution remains gaussian, but the width of the Gaussian is changed according to eq. 4.29.

To the non-statistic broadening we have to add the statistical effects. When the incident beam with initial energy E_0 and initial beam width σ_0^2 (σ^2 is the variance of the energy distribution, the full width at half maximum (FWHM) is $2\sqrt{2\ln 2}\,\sigma = 2.355\,\sigma$) penetrates a layer of matter with thickness Δx, then the beam width σ_1^2 after penetrating the layer is given by:

$$\sigma_1^2 = \left(1 - \frac{d\epsilon}{dE}(E_0)\Delta x\right)^2 \sigma_0^2 + \sigma^2 \tag{4.30}$$

$\epsilon(E) = dE/dx(E)$ is the stopping power of the material and σ^2 is the energy loss straggling in the layer including nuclear energy loss straggling in Bohr approximation and electronic

energy loss straggling according to Chu's theory. The first term in eq. 4.30 describes the non-statistical broadening of the beam according to eq. 4.29 due to the energy dependence of the stopping power, the second term adds the statistical effects.

The variance of the energy loss straggling σ^2 in eq. 4.30 has two contributions: nuclear energy loss straggling σ_n^2 and electronic energy loss straggling σ_e^2. The total straggling σ^2 is given by quadratically adding the two independent contributions of electronic and nuclear straggling:

$$\sigma^2 = \sigma_e^2 + \sigma_n^2 \tag{4.31}$$

The electronic energy loss straggling is calculated by applying Chu's theory [30, 26]:

$$\sigma_e^2 = H(E/M_1, Z_2)\sigma_{Bohr}^2 \tag{4.32}$$

σ_{Bohr}^2 is the electronic energy loss straggling in Bohr approximation and is given by [25, 26]:

$$\sigma_{Bohr}^2\ [\mathrm{keV}^2] = 0.26\, Z_1^2\, Z_2\, \Delta x\ [10^{18}\,\mathrm{atoms/cm}^2] \tag{4.33}$$

Bohr's theory of electronic energy loss straggling is valid in the limit of high ion velocities. In this case the electronic energy loss straggling is almost independent of the ion energy. For lower ion energies the Bohr straggling is multiplied by the Chu correction factor $H(E/M_1, Z_2)$, which depends only on E/M_1 and the nuclear charge of the target atoms Z_2. H takes into account the deviations from Bohr straggling caused by the electron binding in the target atoms. Chu [30, 26] has calculated H by using the Hartree-Fock-Slater charge distribution. This calculation gives straggling values which are considerably lower than those given by Bohr's theory. The correction factor H, as used by SIMNRA, is shown in fig. 4.3. The Z_2 oscillations are clearly visible. The Chu correction is mainly necessary for high Z_2 and low energies. For high energies H approaches 1 and becomes independent of Z_2 and energy. For E/M_1 values in the range 100–1000 keV/amu the data have been taken from ref. [26], data for lower and higher E/M_1 values are based on an extrapolation performed in ref. [20]. Tabulated values for H are stored in the file CHU_CORR.DAT. For not tabulated values SIMNRA uses linear interpolation.

For the nuclear energy loss straggling σ_n^2 SIMNRA uses Bohr's theory of nuclear straggling. The nuclear energy loss straggling in Bohr's approximation is given by:

$$\sigma_n^2\ [\mathrm{keV}^2] = 0.26\, Z_1^2\, Z_2^2 \left(\frac{M_1}{M_1 + M_2}\right)^2 \Delta x\ [10^{18}\,\mathrm{atoms/cm}^2] \tag{4.34}$$

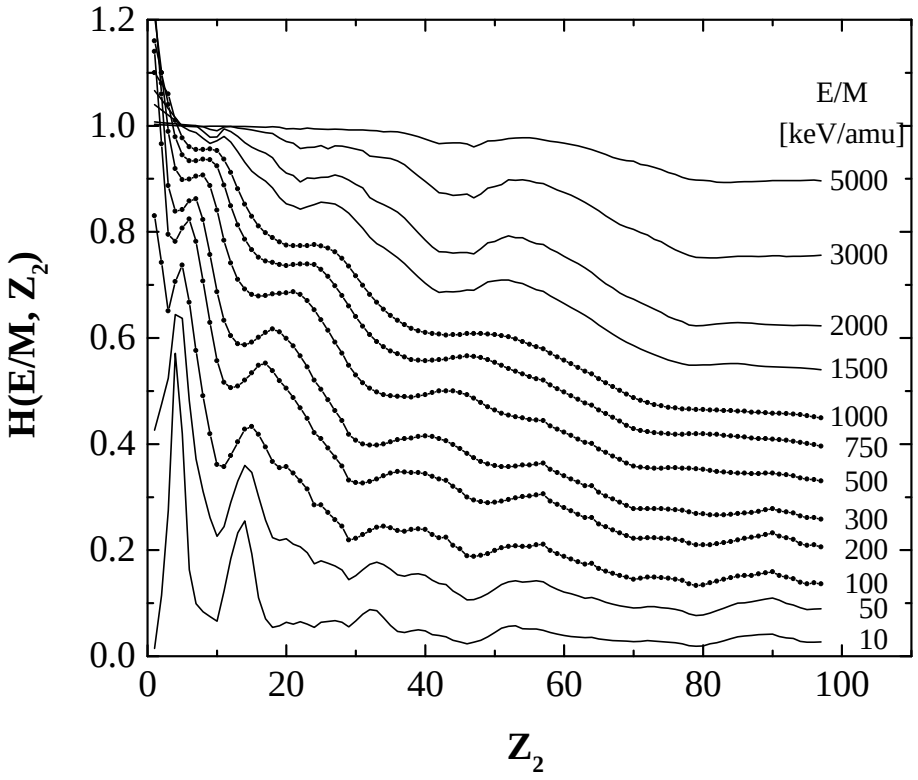

Figure 4.3: The Chu straggling correction for several values of E/M_1 as a function of the nuclear charge of the target Z_2. Dots are original data from Chu [26], solid lines are extrapolated data taken from [20].

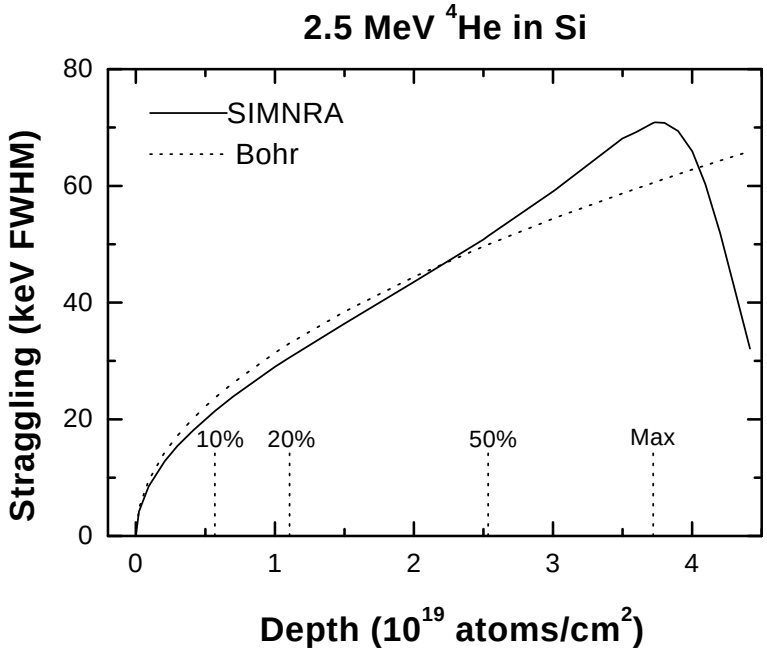

Figure 4.4: Beam width (FWHM) of 2.5 MeV ^{4}He ions penetrating through silicon. The solid line is the beam width calculated by SIMNRA using eq. 4.30, the dashed line is the prediction of Bohr's theory. The vertical lines denote the mean depth at which the beam has lost 10%, 20% and 50% of its initial energy. Max denotes the depth at which the mean energy of the beam has decreased to the energy of the stopping power maximum.

Because the nuclear energy loss straggling is generally much smaller than the electronic energy loss straggling, Bohr's theory of nuclear straggling can be used without loss in precision.

Fig. 4.4 compares the beam width (FWHM) of 2.5 MeV ^{4}He ions in silicon calculated by SIMNRA using eq. 4.30 with Bohr's theory. For small energy losses the beam width calculated by SIMNRA is slightly smaller than predicted by Bohr's theory due to the Chu correction. However, this is counterbalanced by the nonstochastic broadening due to the characteristics of the stopping power curve, and for larger energy losses the beam width gets larger than in Bohr's theory. When the mean beam energy has decreased below the energy of the stopping power maximum, the beam width becomes skewed.

As can be seen from fig. 4.3 the deviation of the Chu correction from Bohr's theory is largest for high Z_2 and low energies. Fig. 4.5 shows the beam width (FWHM) of 1 MeV ^{4}He penetrating through gold. The deviation from Bohr's theory is large. The stopping power maximum is at about 960 keV. For low energy losses the beam width increases due

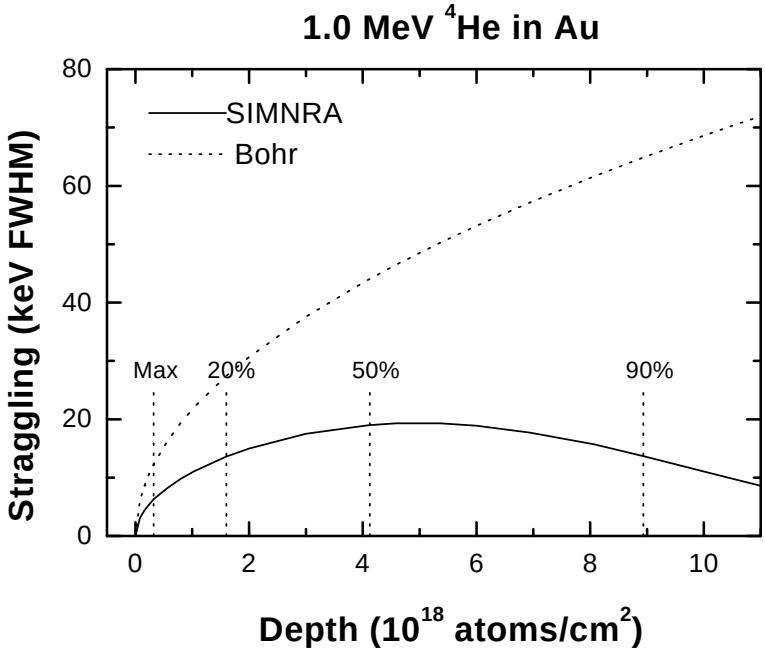

Figure 4.5: Beam width (FWHM) of 1.0 MeV ^{4}He ions penetrating through gold. The solid line is the beam width calculated by SIMNRA using eq. 4.30, the dashed line is the prediction of Bohr's theory. The vertical lines denote the mean depth at which the beam has lost 20%, 50% and 90% of its initial energy. Max denotes the depth at which the mean energy of the beam has decreased to the energy of the stopping power maximum.

to the statistical broadening because the nonstochastic skewing, which occurs for beam energies below the stopping power maximum, is small and the stochastic broadening wins. For larger energy losses however the beam width gets skewed.

Fig. 4.6 shows the measured RBS-spectrum for 1.0 MeV ^{4}He ions incident on a gold layer with a thickness of about 100 nm and a scattering angle of 165° compared with simulations using Bohr straggling and Chu straggling. As can be seen at the low energy edge of the layer, the Bohr straggling is broader than the experimental data. The Chu straggling fits the measured curve relatively well, except of the multiple scattering contribution.

The straggling of outgoing particles is calculated with eq. 4.30 as well. Outgoing particles always start with an energy distribution with variance σ^2_{out} which is given by

$$\sigma^2_{\text{out}} = K^2\,\sigma^2_{\text{in}} \tag{4.35}$$

with K the kinematic factor and σ^2_{in} the variance of the energy distribution of the incident beam.

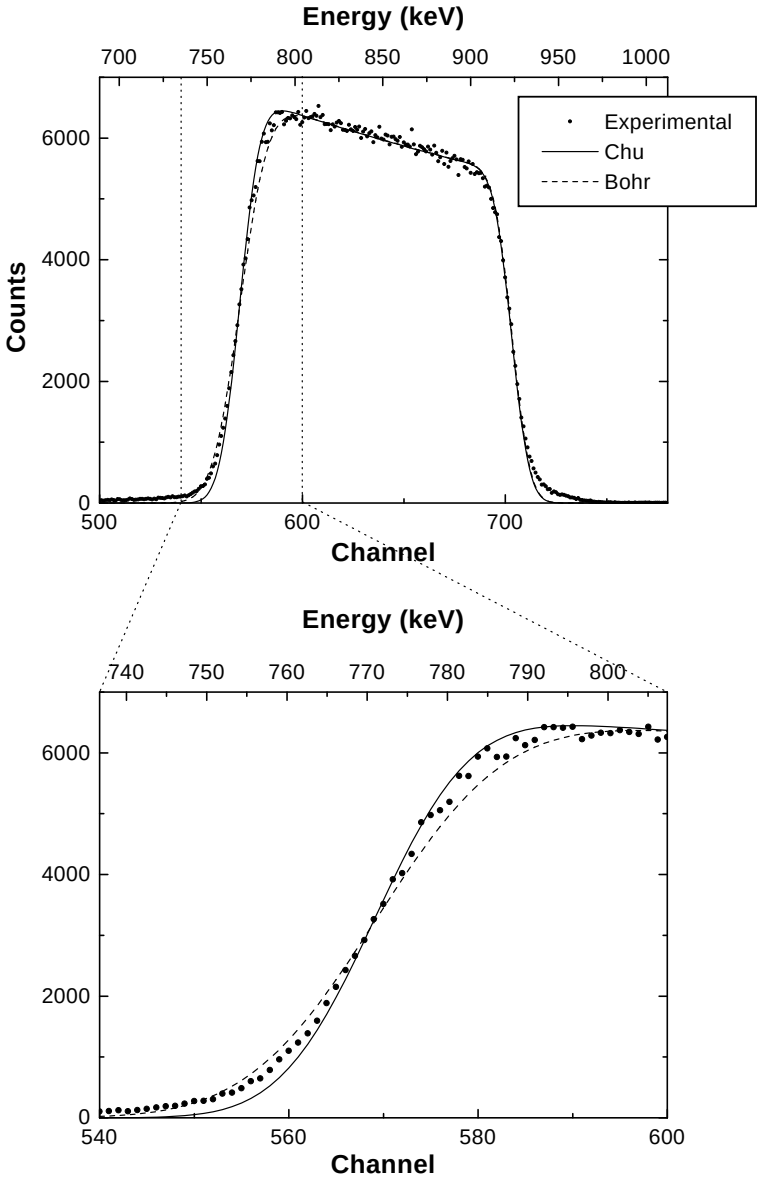

Figure 4.6: Measured and simulated spectra using Bohr and Chu straggling of 1.0 MeV ^{4}He ions incident on 100 nm Au on Si, scattering angle 165°. Bottom: Magnification of the low energy gold edge.

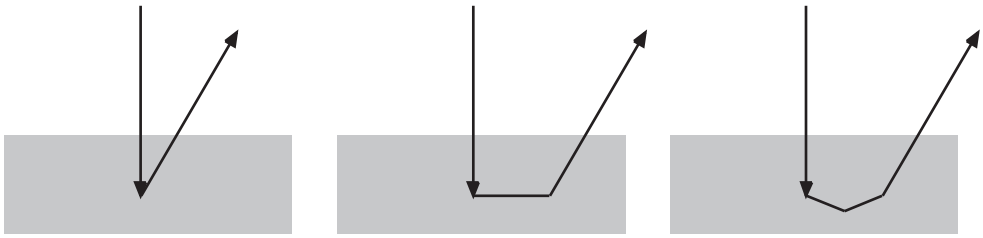

Figure 4.7: Examples of ion trajectories with one, two and three scattering events.

4.5.2 Energy loss straggling in compounds

For compounds a simple additivity rule for energy loss straggling is used [26]. The straggling in a compound consisting of elements i with atomic concentration c_i is calculated with

$$\sigma^2 = \sum_i c_i \, \sigma_i^2 \tag{4.36}$$

with σ_i^2 being the straggling in each element.

4.6 Multiple and plural scattering

SIMNRA uses straight lines as trajectories for the ingoing and outgoing particles, with one single scattering event connecting the trajectories of the particles, see fig. 4.7 left. This is only an approximation to physical reality, because the particles on the ingoing and outgoing path suffer many small angle scatterings with small scattering angles (this has been called multiple scattering) and additionally may perform more than one scattering event with large scattering angle (see fig. 4.7 middle and right), before they are scattered towards the detector. This has been called plural scattering.

Multiple scattering has been recently reviewed by Szilagy *et al.* [20]. Multiple scattering results in an angular spread of the particles and therefore in a spread of path lengths. Due to the path length differences, we get an energy spread of the particles in a given depth. Multiple scattering is not treated by SIMNRA.

Plural scattering with 2, 3, 4, ... scattering events is responsible for the background behind the low energy edge of high Z elements on top of low Z elements and the steeper increase of the spectra towards low energies than calculated with single scattering [31, 32]. SIMNRA is able to calculate dual scattering, i. e. all particle trajectories with two scattering events.

SIMNRA performs the calculation of dual scattering in the following way: During each step of the incident ion particles are scattered into the whole sphere of 4π. We introduce the polar system with the polar angles ψ, ϕ, see fig. 4.8. After the first scattering event the scattered particles have the direction ψ, ϕ. The scattering angle θ_1 of the first scattering event is given by

$$\cos\theta_1 = \sin\alpha\ \sin\psi\ \sin\phi - \cos\alpha\ \cos\psi$$

SIMNRA uses the Rutherford cross-section for the calculation of the number of scattered particles in the first scattering event. The new angle α' of the particles after the first scattering is

$$\alpha' = 180^\circ - \psi$$

The scattering angle θ_2 of the second scattering event is given by

$$\cos\theta_2 = \sin\beta\ \sin\psi\ \sin\phi + \cos\beta\ \cos\psi$$

SIMNRA subdivides the whole sphere of 4π into 10 ψ-intervals and 12 ϕ-intervals, resulting in 120 solid angle intervals. SIMNRA considers only trajectories with scattering angles $\theta_1, \theta_2 > 20^\circ$ for dual scattering. Trajectories with smaller scattering angles are very similar to single scattering trajectories. For each solid angle interval a full backscattering spectrum with the starting depth of the particles equal to the depth of the incident ions and the new incident angle α' and the new scattering angle θ_2 is calculated.

Fig. 4.9 compares the simulated spectra with single and dual scattering for 500 keV ^{4}He ions incident on a 100 nm gold layer on top of silicon with experimental data. With the inclusion of dual scattering the experimental results are much better approximated. Dual scattering gives the background between the low energy edge of Au and the Si edge, and the steeper increase of the gold spectrum is better described. The results with dual scattering are slightly lower than the experimental results. This is due to trajectories with more than two scattering events.

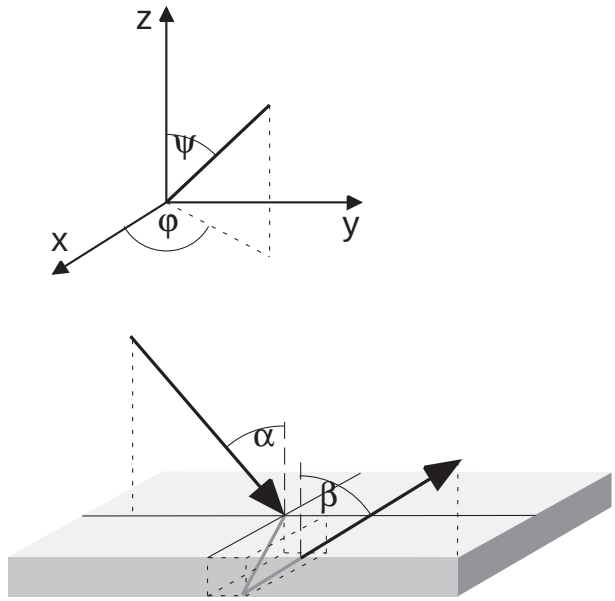

Figure 4.8: Geometry used for the calculation of dual scattering.

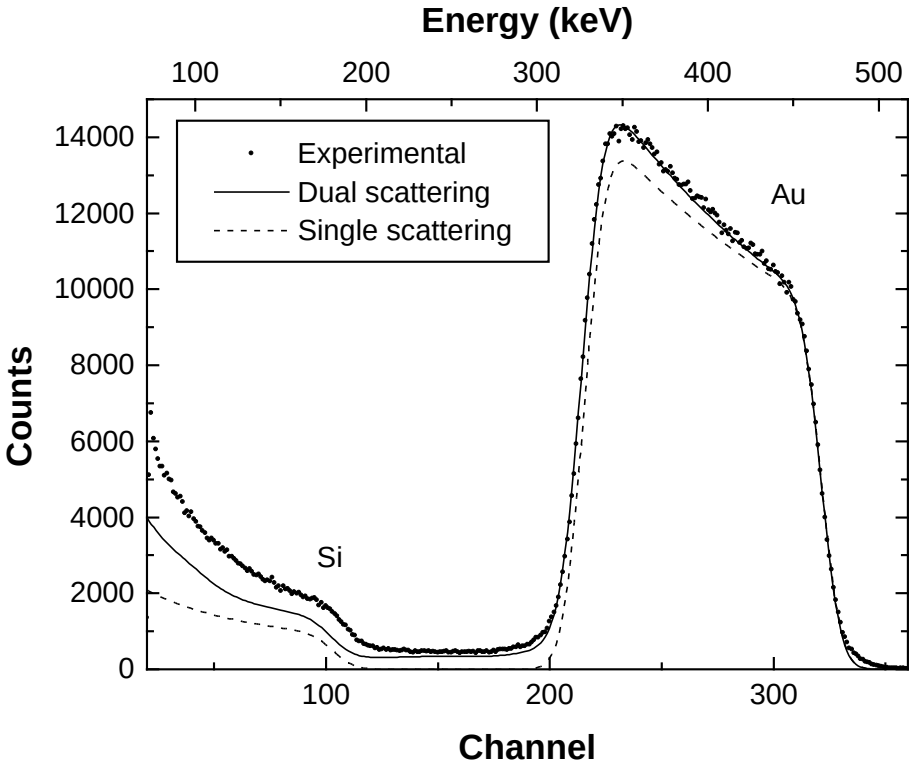

Figure 4.9: 500 keV ^{4}He ions incident on 100 nm Au on top of Si, scattering angle 165°. Circles: experimental data points, dashed line: simulation with one scattering event, solid line: simulation with two scattering events.

Chapter 5

Examples

This chapter gives several examples for the abilities of SIMNRA.

All backscattering spectra were measured at the IPP Garching at a scattering angle $\theta = 165°$. The solid angle of the detector was 1.08×10^{-3} sr. A standard surface barrier detector with a nominal energy resolution of 15 keV FWHM was used.

5.1 RBS: Rutherford cross-sections

Fig. 5.1 shows the measured and simulated spectra for 1.0 MeV ^{4}He incident ions on a gold layer with a thickness of about 100 nm on top of silicon. The simulated spectrum fits the measured data very well. The low background between the Si edge and the low energy Au edge is due to plural scattering (this means the backscattered particles have suffered more than one scattering event with large scattering angle) [31, 32], which was not simulated for this example. The deviation between experiment and simulation at low energies in the Si spectrum is due to the same reason.

Fig. 5.2 compares simulated spectra with single and dual scattering for 500 keV ^{4}He ions incident on a 100 nm gold layer on top of silicon with experimental data. At this low energy plural scattering is important. With the inclusion of dual scattering the experimental results are much better approximated. Dual scattering gives the background between the low energy edge of Au and the Si edge, and the steeper increase of the gold spectrum is better described. The results with dual scattering are slightly lower than the experimental results. This is due to trajectories with more than two scattering events, which are not calculated.

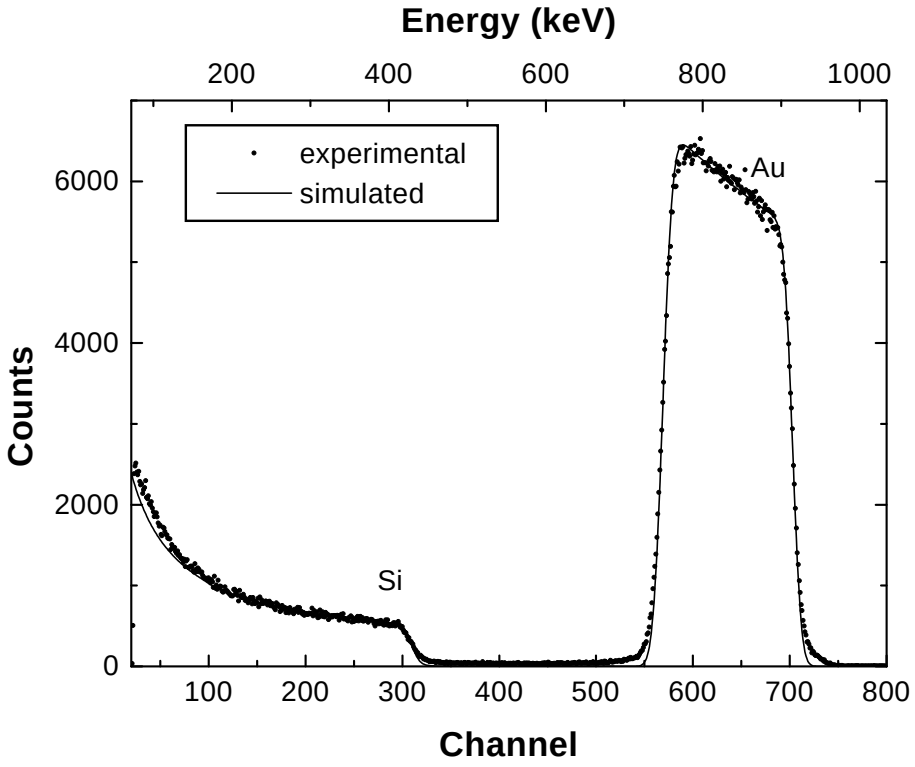

Figure 5.1: 1000 keV ^{4}He incident on Au on top of silicon, $\theta = 165°$.

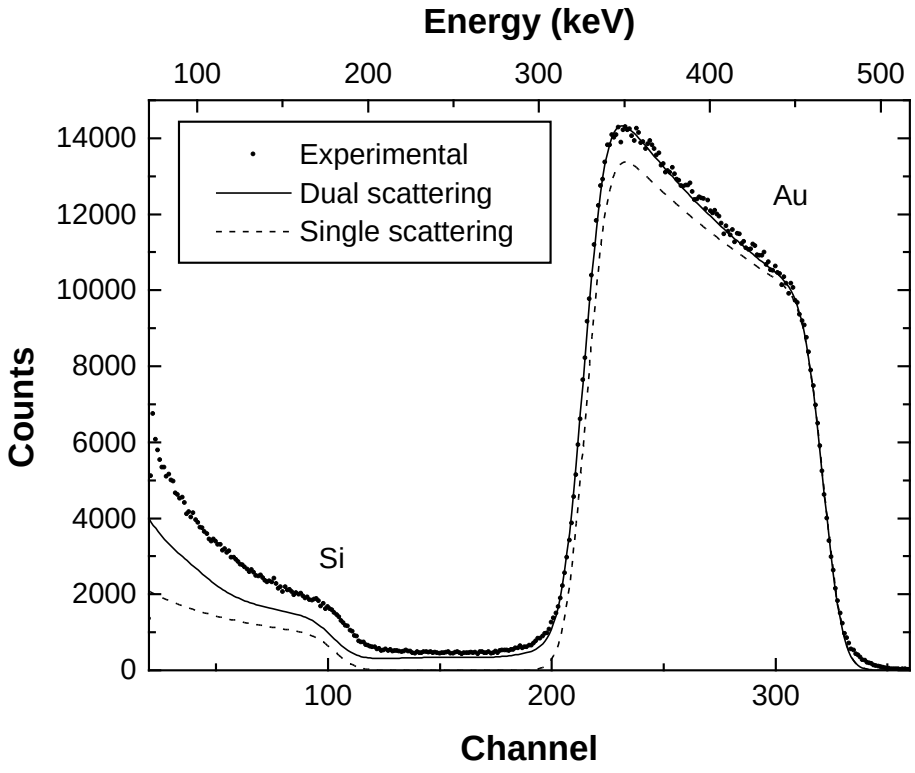

Figure 5.2: 500 keV ^{4}He ions incident on 100 nm Au on top of Si, scattering angle 165°. Circles: experimental data points, dashed line: simulation with one scattering event, solid line: simulation with two scattering events.

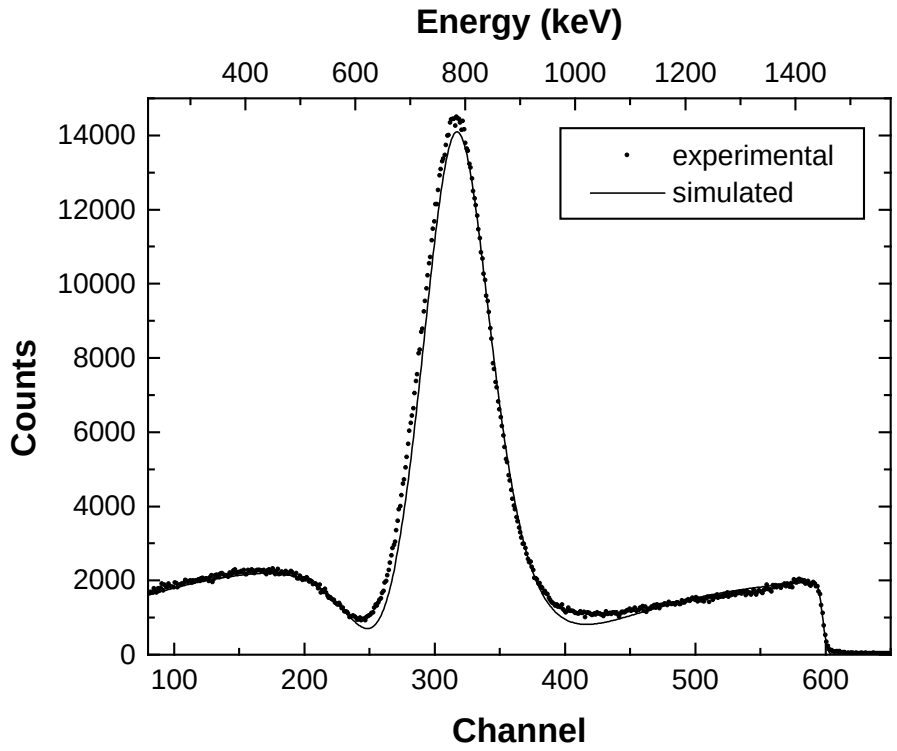

Figure 5.3: 2000 keV protons on carbon (HOPG), $\alpha = 5°$, $\theta = 165°$.

5.2 RBS: Non-Rutherford cross-sections

Fig. 5.3 shows the measured and simulated spectra for 2.0 MeV protons incident on highly oriented pyrolytic graphite (HOPG). To avoid channelling the incident angle α was 5°. The cross-section is non-Rutherford, and the cross-section data of Amirikas *et. al.* [33] were used for the simulation. The pronounced peak in the spectrum is due to the resonance in the ^{12}C(p,p)^{12}C cross-section at 1732 keV. The measured and simulated spectra agree very well.

Fig. 5.4 shows the measured and simulated spectra for 2.0 MeV protons incident on silicon. To avoid channelling the incident angle α was 5°. The cross-section is non-Rutherford, and the cross-section data of Vorona *et. al.* [34] were used for the simulation. As in the case of carbon the measured and simulated spectra agree very well. The structures in the simulated spectrum between channel 500 and 700 are due to the experimentally determined cross-section data, which contain these structures.

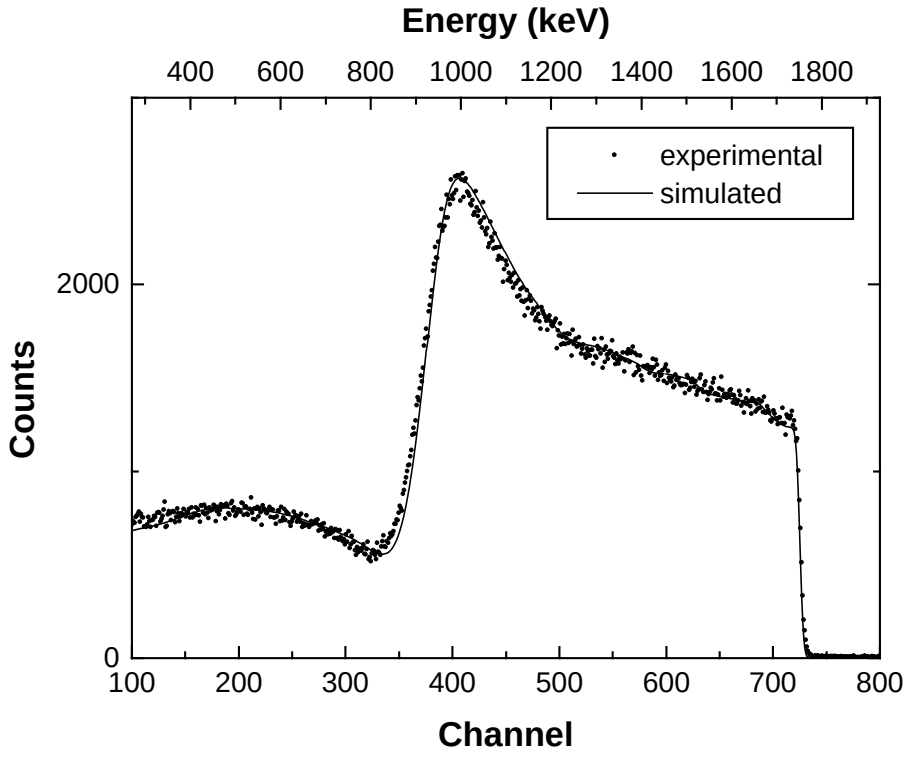

Figure 5.4: 2000 keV protons backscattered from silicon, $\alpha = 5°$, $\theta = 165°$.

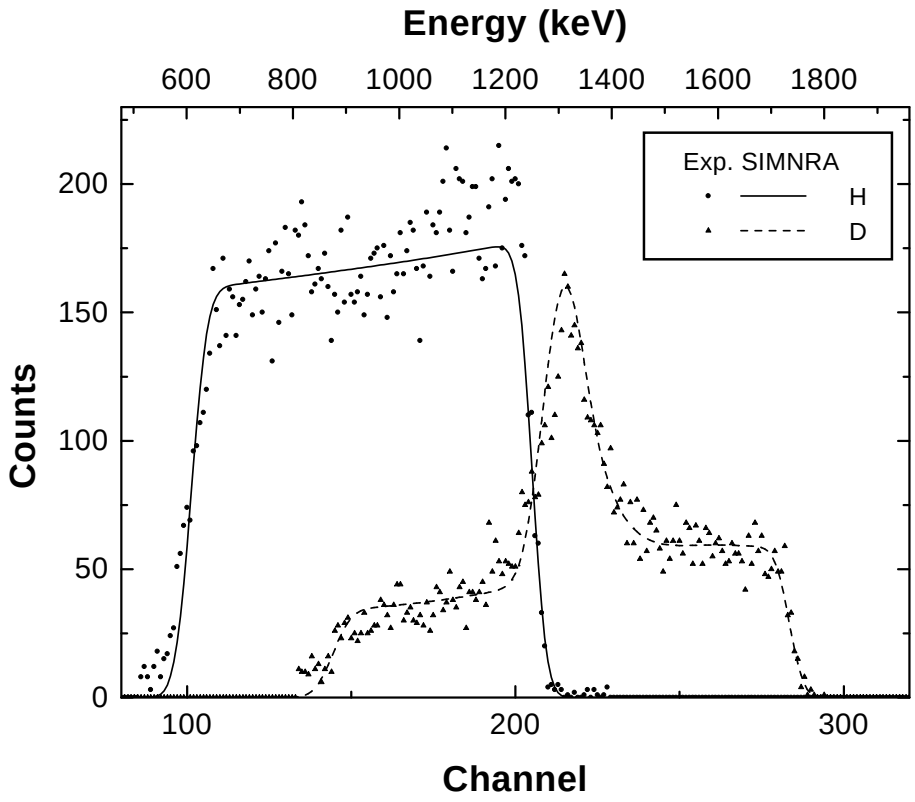

Figure 5.5: ERDA with 2.6 MeV ^{4}He ions incident on a soft amorphous hydrocarbon layer (a:C-H layer) containing both H and D. The recoiling H and D atoms were separated with a ΔE-E telescope detector, the backscattered ^{4}He ions are not shown. $\alpha = \beta = 75°$, $\theta = 30°$.

5.3 ERDA: Non-Rutherford cross-sections

Fig 5.5 shows the measured and simulated spectra for ERDA with 2.6 MeV incident ^{4}He ions on a soft amorphous hydrocarbon layer (a:C-H layer) containing both H and D. The recoiling H and D atoms were separated with a ΔE-E telescope detector [35]. Both recoil cross-sections are non-Rutherford. The cross-section data of Baglin *et al.* [36] for H(^{4}He,H)^{4}He and of Besenbacher *et al.* [37] for D(^{4}He,D)^{4}He were used for the simulation. The peak in the deuterium spectrum is due to a resonance at a ^{4}He energy of 2130 keV. The measured and simulated data agree very well.

Bibliography

[1] J.R. Tesmer and M. Nastasi, Eds. *Handbook of Modern Ion Beam Materials Analysis*. Materials Research Society, Pittsburgh, Pennsylvania, 1995.

[2] M.S. Caceci and W.P. Cacheris. Byte, 5 (1984) 340.

[3] W. Hösler and R. Darji. Nucl. Instr. Meth. B85 (1994) 602.

[4] E. Steinbauer, P. Bauer, M. Geretschläger, G. Bortels, J.P. Biersack, and P. Burger. Nucl. Instr. Meth. B 85 (1994) 642.

[5] R. Doolittle. Nucl. Instr. Meth. B9 (1985) 344.

[6] R. Doolittle. Nucl. Instr. Meth. B15 (1986) 227.

[7] J. L'Ecuyer, J.A. Davies, and N. Matsunami. Nucl. Instr. Meth. 160 (1979) 337.

[8] M. Hautala and M. Luomajärvi. Rad. Effects 45 (1980) 159.

[9] H.H. Andersen, F. Besenbacher, P. Loftager, and W. Möller. Phys. Rev. A21, 6 (1980) 1891.

[10] M. Bozoian, K.M. Hubbard, and M. Nastasi. Nucl. Instr. Meth. B51 (1990) 311.

[11] M. Bozoian. Nucl. Instr. Meth. B58 (1991) 127.

[12] M. Bozoian. Nucl. Instr. Meth. B82 (1993) 602.

[13] H.H. Anderson and J.F. Ziegler. *Hydrogen - Stopping Powers and Ranges in All Elements*, vol. 3 of *The Stopping and Ranges of Ions in Matter*. Pergamon Press, New York, 1977.

[14] J.F. Ziegler. *Helium - Stopping Powers and Ranges in All Elements*, vol. 4 of *The Stopping and Ranges of Ions in Matter*. Pergamon Press, New York, 1977.

[15] J.F. Ziegler. *Stopping Cross-Sections for Energetic Ions in all Elements*, vol. 5 of *The Stopping and Ranges of Ions in Matter*. Pergamon Press, New York, 1980.

[16] J.F. Ziegler, J.P. Biersack, and U. Littmark. *The Stopping and Range of Ions in Solids*, vol. 1 of *The Stopping and Ranges of Ions in Matter*. Pergamon Press, New York, 1985.

[17] W.H. Bragg and R. Kleeman. Philos. Mag. 10 (1905) 318.

[18] D. Boutard, W. Möller, and B.M.U. Scherzer. Phys. Rev. B38, 5 (1988) 2988.

[19] J.F. Ziegler and J.M. Manoyan. Nucl. Instr. Meth. B35 (1988) 215.

[20] E. Szilágy, F. Pászti, and G. Amsel. Nucl. Instr. Meth. A4, B100 (1995) 103.

[21] M.A. Kumakhov and F.F. Komarov. *Energy Loss and Ion Ranges in Solids.* Gordon and Breach Science Publishers, New York, London, Paris, 1981.

[22] J.R. Bird and J.S. Williams, Eds. *Ion Beams for Materials Analysis.* Academic Press, Sydney, New York, Tokyo, 1989.

[23] J. Tirira, Y. Serruys, and P. Trocellier. *Forward Recoil Spectrometry.* Plenum Press, New York, London, 1996.

[24] P.V. Vavilov. Soviet Physics J.E.T.P. 5 (1957) 749.

[25] N. Bohr. Mat. Fys. Medd. Dan. Vid. Selsk. 18, 8 (1948) .

[26] J.W. Mayer and E. Rimini. *Ion Handbook for Material Analysis.* Academic Press, New York, San Francisco, London, 1977.

[27] M.G. Payne. Phys. Rev. 185, 2 (1969) 611.

[28] C. Tschalär. Nucl. Instr. Meth. 61 (1968) 141.

[29] C. Tschalär. Nucl. Instr. Meth. 64 (1968) 237.

[30] W.K. Chu. Phys. Rev. 13 (1976) 2057.

[31] E. Steinbauer, P. Bauer, and J.P. Biersack. Nucl. Instr. Meth. B 45 (1990) 171.

[32] P.Bauer, E. Steinbauer, and J.P. Biersack. Nucl. Instr. Meth. B79 (1993) 443.

[33] R. Amirikas, D.N. Jamieson, and S.P. Dooley. Nucl. Instr. Meth. B77 (1993) 110.

[34] J. Vorona, J.W. Olness, W. Haeberli, and H.W. Lewis. Phys. Rev. 116 (1959) 1563.

[35] M. Wielunski, M. Mayer, R. Behrisch, J. Roth, and B.M.U. Scherzer. Nucl. Instr. Meth. B122 (1997) 113.

[36] J.E.E. Baglin, A.J. Kellog, M.A. Crockett, and A.H. Shih. Nucl. Instr. Meth. B64 (1992) 469.

[37] F. Besenbacher, I. Stensgaard, and P. Vase. Nucl. Instr. Meth. B15 (1986) 459.